The Abdus Salam
International Centre for Theoretical Physics

United Nations
Educational, Scientific and
Cultural Organization

IAEA
International Atomic Energy Agency

2141-17

Joint ICTP-IAEA Workshop on Nuclear Reaction Data for Advanced Reactor Technologies

3 - 14 May 2010

RIPL-3 and uncertainties of model parameters

IGNATYUK Anatoly
IPPE
Obninsk
RUSSIAN FEDERATION

RIPL-3 and uncertainties of model parameters

A.V.Ignatyuk
Institute of Physics and Power Engineering, Obninsk, Russia

Abstract: Modern advance-modelling codes require a considerable amount of numerical input. To meet nowadays needs the International Atomic Energy Agency (IAEA) has incited extensive efforts to develop a library of validated nuclear-model input parameters, referred to as the Reference Input Parameter Library (RIPL). The current status of the library is briefly reviewed in the present lecture.

Our theoretical understanding of low-energy nuclear reactions induced by light particles has reached a reasonable degree of reliability, and nuclear modelling codes are widely used to assess and guide nuclear data evaluations (with measurements remaining crucial for data testing and benchmarking). Such codes require a considerable amount of numerical input and a research activity was started in 1993 by IAEA to develop a library of validated nuclear-model input parameters. A final RIPL coordinated research project on "Parameters for Calculation of Nuclear Reactions of Relevance to Non-Energy Nuclear Applications" (RIPL-3) was brought to a successful conclusion in December 2008, after 15 years of challenging work carried out through three consecutive IAEA coordinated research projects.

The RIPL-3 library was released in January 2009, and is available on the Web through *http://www-nds.iaea.org/RIPL-3/*. This work and the resulting database are extremely important to theoreticians involved in the development and use of nuclear reaction modelling codes (e.g. ALICE, EMPIRE, GNASH, UNF and TALYS) both for theoretical research and nuclear data evaluations.

The numerical data and computer codes included in RIPL-3 are arranged in seven segments: **atomic masses, low-lying discrete levels, neutron resonance parameters, optical model parameters, nuclear level densities, gamma-ray strength functions, and nuclear fission parameters.**

The content of the IAEA Reference Input Parameter Library are briefly reviewed in this lecture with a special attention to uncertainties of model parameters. A more complete description of the library is presented in Refs. [1-4].

ATOMIC MASSES

Mass, or binding energy, is one of the most fundamental properties of atomic nuclei. A large number of processes in nuclear physics require for their description an accurate knowledge of nuclear masses. Mass predictions are, for example, a critical element of many calculations required in nuclear astrophysics. Mass values also define nuclear reaction thresholds and Q-values. Many different mass formulae are available nowadays. However, we consider in RIPL only global approaches which provide predictions of nuclear masses for all nuclei up to the super-heavy region $Z < 120$ lying between the proton and the neutron drip lines.

The RIPL mass segment consists of a combined set of experimental values, along with three theoretical predictions of masses and deformations.

Experimental masses

The mass $M_{nuc}(N,Z)$ of a nucleus with N neutrons (of mass M_n) and Z protons (of mass M_p) is measurably different from the sum of the masses of the free nucleons, and provides a direct determination of the internal energy E_{nuc} (negative of the binding energy) of the nucleus:

$$E_{nuc} = (M_{nuc}(N,Z) - NM_n - ZM_p)\, c^2. \qquad (1)$$

The latest compilation of experimental atomic masses corresponds to the 2003 publication of Audi *et al.* [5] and includes 2228 nuclei. They also estimated a set of 951 additional masses from trends in systematics based on the regularity of the mass surface. The final set of Audi *et al.* best-recommended masses includes 3179 nuclei. The uncertainty associated with each experimental or best-recommended mass is also provided by Audi *et al.*, and is included in the library.

Finite-Range-Droplet-Model masses

Attempts to develop formula or more generally algorithms representing the variation in E_{nuc} from one nucleus to another go back to the 1935 "semi-empirical mass formula" of von Weizseacker. This approach corresponds to the widely used liquid-drop model (LDM) of the nucleus, i.e. macroscopic mass formula that accounts for all but a small part of the variation in the binding energy. Improvements have been gradually made to the original liquid-drop mass formula, leading to the development of macroscopic-microscopic mass formula, where microscopic corrections to account for the shell and pairing correlation effects are added to the liquid drop part. The macroscopic and microscopic features are treated independently, both being connected exclusively by a parameter fit to the experimental masses. Later developments include macroscopic properties of infinite and semi-infinite nuclear matter and the finite range character of nuclear forces. The most sophisticated version of this macroscopic-microscopic mass formula is the "finite-range droplet model" [7]. The atomic mass excesses and nuclear ground-state deformations are tabulated for 8979 nuclei ranging from 16O to (Z = 136,A = 339) nucleus. Calculations are based on the finite-range droplet macroscopic model and the folded-Yukawa single-particle microscopic correction. Relative to the 1981 version, improvements are found mainly in the macroscopic model, pairing model with a new form for the effective interaction pairing gap, and minimization of the ground state energy with respect to additional shape degrees of freedom. Parameters are determined directly from a least-squares adjustment to the ground-state masses of 1654 nuclei ranging from 16O to 263Sg. The *rms* deviation is 0.656 MeV for the 2149 $Z,N > 8$ nuclei with experimental masses.

Data file *masses/mass-frdm95.dat* includes the Audi *et al.* (2003) experimental and best recommended masses when available [5], the FRDM calculated masses, microscopic corrections and β-deformation parameters [6]. The microscopic correction *Emic* corresponds to the difference between the total binding energy and the spherical macroscopic energy. Additionally, FDRM single-particle level schemes corresponding to the ground-state deformation of the nucleus are also included in the database. These single-particle levels could be used in the level-density microscopic calculations.

Hartree-Fock-Bogoliubov masses

Microscopic theories based on nucleonic interactions have also been used to estimate the binding energies. One of the most promising microscopic approaches is the non-relativistic Hartree-Fock-Bogoliubov (HFB) method based on an effective nucleon-nucleon interaction of Skyrme type. HFB calculations in which a Skyrme force is fitted to essentially all the mass data [5] are not only feasible, but can also compete with the most accurate droplet-like formulae available as shown in Refs. [7, 8]. The Skyrme HFB mass model not only seeks optimized fits to the mass data, but also allows constructing a universal effective interaction capable of reproducing most of the observables of relevance in nuclear applications.

In RIPL-2, the HFB-2 mass model [9] was recommended. It represents one of the very first microscopic mass models based on the Skyrme-HFB method. HFB-2 reproduces the 2149 experimental masses with an *rms* deviation of 0.659 MeV, but with the drawback of being characterized by a rather strong pairing force and a rather poor description of nuclear and neutron matter properties. Since development of the HFB-2 mass model, improvements have been made to reproduce additional

observables, including in particular infinite nuclear matter properties, as well as nuclear level densities and fission barriers.
The HFB-14 model [7, 8], included in the RIPL-3 library, was subjected to the following constraints: i) energy-density curve of neutron matter was fitted, a requirement that is relevant not only to neutron-star applications, but also to the reliability of finite-nucleus extrapolations out towards the neutron drip line; ii) the strength of the pairing force was held considerably below the value that would emerge from an optimal fit to the mass data, thereby improving considerably the predictions for level densities ; iii) a vibrational term was added to the phenomenological collective correction, fitting this parameter to measured fission-barrier heights. 52 primary fission barriers lower than 9 MeV, which were compiled in the RIPL-2 database, are reproduced with *rms* deviation of 0.67 MeV and the 45 secondary barriers with *rms* deviation of 0.65 MeV. The resulting HFB-14 mass model is characterized by *rms* deviation of 0.729 MeV with respect to the Audi *et al.* (2003) mass data. In addition, the HFB-14 quadrupole moments, charge radii and chargedensity distributions have been shown to be in excellent agreement with experiment.
The complete HFB-14 mass table is available in the *masses/mass-hfb14.dat* file. Along with the Audi *et al.* (2003) experimental and best recommended masses (when available), this table also includes the HFB masses, the β-deformation parameters, and the parameters describing the *n* and *p* density distribution for all 8508 nuclei lying between the two drip lines over the range $Z,N > 8$ and $Z < 110$.

Duflo-Zuker mass formula based on shell model
Another microscopically rooted approach worth considering is the development by Duflo and Zuker [10] of a mass formula based on the shell model. The nuclear Hamiltonian is separated into a monopole term and a residual multipole term: the monopole term is responsible for saturation and single-particle properties, and fitted phenomenologically; multipole part is derived from realistic interactions. The latest version of the mass formula defined in terms of 10 free parameters reproduces the 2149 $Z,N > 8$ experimental masses with an outstanding *rms* uncertainty of 0.564 MeV. A simple 120-lines FORTRAN subroutine in the *masses/duflozuker96. f* file computes the mass of any nucleus with ease, especially when relevant data are not available in the above-mentioned tables.

Shell corrections
Microscopic corrections to the binding energy are quantities of fundamental importance in the derivation of many physical properties affected by shell, pairing or deformation effects. Different definitions exist. The most common one defines the various microscopic corrections as follows:

$$E_{tot}(Z, A,\beta) = E_{mac}(Z, A, \beta) + E_{shell}(Z, A, \beta), \quad (2)$$

where β characterizes the nuclear shape at equilibrium, E_{mac} is the smooth macroscopic similar to the liquid-drop model energy and E_{shell} is the shell-plus-pairing correction energy (we define the pairing correction for even-even nuclei and do not consider the odd-even effect).
Each mass model calls for specific theoretical calculations to estimate the macroscopic part, as well as the shell, pairing and deformation energies. The most common approaches to derive the macroscopic part are the Finite-Range Droplet or Liquid Drop model [6], the Thomas-Fermi approach [11], or the Extended-Thomas- Fermi approach [12]. Depending on the approach followed to derive the smooth macroscopic part of the binding energy and the parameter set adopted for the macroscopic part, the microscopic corrections can take relatively different values. The FRDM microscopic correction E_{mic} can be found in the *masses/mass-frdm95.dat* file. As an example the shell corrections estimated by different authors are shown in Fig. 1 for the stable nuclei for which the experimental data on neutron resonance densities are available.

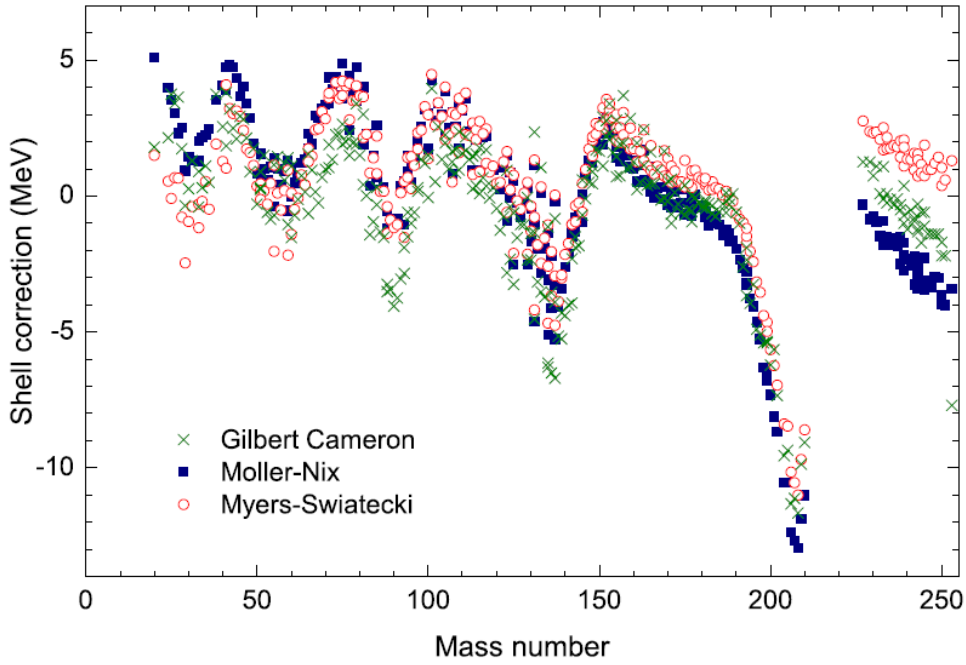

Fig. 1. Shell corrections to the nuclear binding energies estimated by different authors.

Uncertainties in the mass predictions

The uncertainties associated with the mass predictions come from uncertainties affecting either the model parameters or the model itself. Within the macroscopic-microscopic model, the deviations related to the model parameters are known to be potentially very large. As far as the HFB mass models are concerned, they have been shown to be relatively stable with respect to changes of the force parameters, at least if the force is fitted to essentially all experimental mass data [8]. Globally, the extrapolations out to the neutron drip-line of the different HFB mass models are essentially equivalent, with deviations up to typically 5 MeV being found.

However, major differences between the droplet-like, the Duflo-Zuker and HFB models still exist, not only in the prediction of nuclear masses located some distance from the experimentally known region, but also in the strength of the shell and pairing effects. The model uncertainties still affecting the nuclear mass predictions are therefore well illustrated by the mass differences between the three models recommended as shown in Fig. 2. Despite the close similarity in the quality of the fits to the data given by these different models, large differences emerge as the neutron-drip line is approached.

DISCRETE LEVEL SCHEMES

Nuclear reaction and statistical model calculations require complete knowledge of nuclear level schemes for specifying all possible outgoing reaction channels. Knowledge of discrete levels is also important for adjusting level densities, which replace unknown discrete level schemes at higher excitation energies where the discrete levels become too dense to be resolved. For this purpose the estimate of the completeness of the level scheme is of crucial importance. The term “completeness ” means that up to a certain excitation energy all discrete levels in a given nucleus are observed and are characterized by unique energy, spin and parity values. The knowledge of particle and gamma-ray decay branchings from each level is also required, especially when population of isomeric states is of interest.

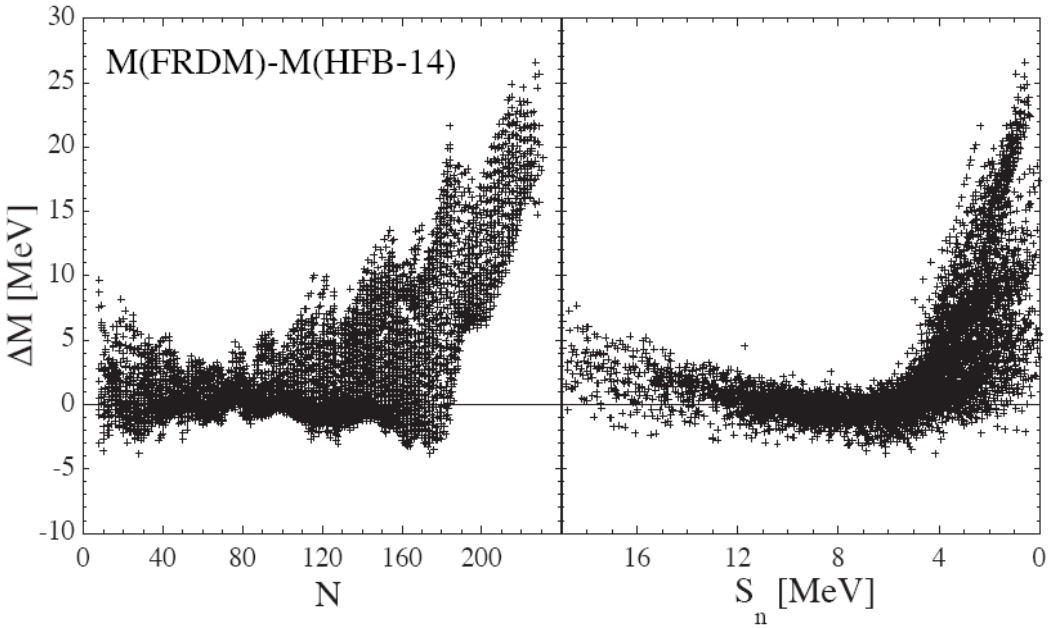

FIG. 2: Differences between the FRDM and HFB-14 mass predictions as a function of neutron number N (left) and the HFB-14 neutron separation energy S_n (right).

The first attempt to create a sublibrary of discrete levels for applications was undertaken in the RIPL-1 project. The RIPL-1 starter file [1], however, suffered from a number of deficiencies related to the use of the retrieval code and a too restrictive format. Therefore, a new, extended Discrete Level Schemes (DLS) sublibrary was created during the RIPL-2 project [2]. The sublibrary was created by the Budapest group using the ENSDF-II data set of 1998 as a source.

One of the most difficult tasks was the determination of the maximum level number N_{max}, and the corresponding cut-off energy E_{max}, up to which a level scheme is supposed to be complete. It is well known that the observed energy dependence of the cumulative number of levels $N(E)$ as a function of excitation energy E can be described rather well by the empirical function

$$N(E) = \exp\left[(E - E0)/T\right] \quad , \qquad (3)$$

where $E0$ and T are free parameters determined by fitting corresponding data. Since the value of this parameter is assumed to be constant over the energy range considered, Eq. (3) is called the constant temperature level-density model. When we are using Eq. (3) to fit the low-lying discrete levels we usually skip the first few levels (especially in even-even nuclei), so the fit goes from N_{min} to N_{max} level number. In each iteration of the fitting process the N_{max} and N_{min} level numbers for each nucleus are varied independently, in such a way that the fit approaches the part of the level scheme that can be well described by the constant temperature formula. The resulting N_{max} values have been identified as the level number up to which the level schemes can be considered complete.

The temperature T as a function of the mass number A was obtained from a global least-squares fit for 625 nuclei, which were defined as ±4 mass-unit band around the valley of stability. An additional 503 nuclei that were not used in the global fit have been fitted using the above determined $T(A)$ function in order to estimate N_{max} values. The obtained values of T and the shift parameters E_0 together with the corresponding uncertainties are shown in Figs. 3 and 4 as a function of the mass number A. We can see that E_0 is positive for even-even and negative for odd-odd nuclei, and fluctuates between positive and negative numbers for odd nuclei. The mass dependence of nuclear temperature is rather smooth with some well-marked increases for the magic numbers of neutrons.

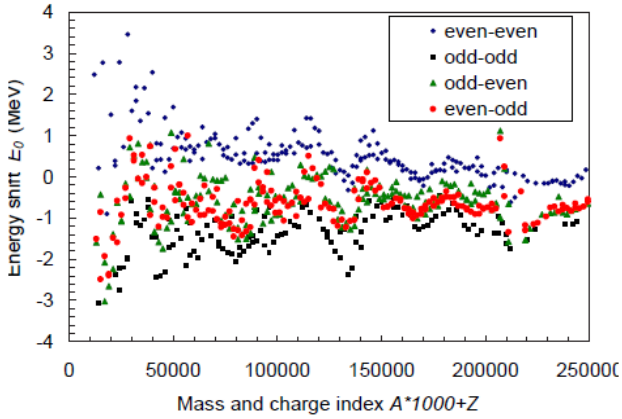

Fig.3. Shift parameter E_0 as a function of mass number.

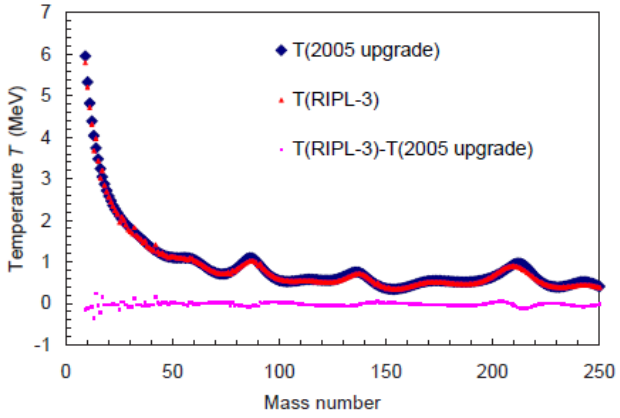

Fig. 4. Nuclear temperature fits in the 2007 sublibrary (red) relative to the 2005 sublibrary (blue).

The major steps in the construction of the DLS sublibrary were the following:

• Adopted or available discrete nuclear levels and gamma-ray transitions from ENSDF have been retrieved and converted into RIPL format using FORTRAN programs developed within the CRP.

• Cut-off energies E_{max}, and the corresponding cumulative numbers of levels N_{max}, have been determined from a constant-temperature fitting procedure to the staircase plots for nuclei with at least 20 known levels as described above.

• Additional energy cut-offs E_c, corresponding to the energy of the highest level with unique spin and parity assignment, have been determined for all nuclei on the basis of the ENSDF data alone.

• Data retrieved from the ENSDF have been extended in order to obtain unique data values as required for reaction calculations. To this end, unique spin and parity values have been generated from known data up to the cut-off energy E_{max}. Internal conversion coefficients (ICC) for electromagnetic transitions have been calculated using unique spin and parity values if they were not given in the ENSDF. The extension has included the complete decay pattern of the levels if known from experiments.

• Data have been tested for internal inconsistencies, which could be due to misprints, logical errors, or use of improper algorithms.

• For nuclei that had at least 10 levels with spin assignment below N_{max}, the spin cutoff factors have been calculated from the spin assignments provided in the ENSDF.

• Missing spins and parities have been inferred up to N_{max}.

The first update of the RIPL-2 DLS sublibrary was undertaken in 2005 and the second one was performed in late 2007. Minor modifications of the software were necessary to handle some new features found in the ENSDF library. The RIPL-3 sublibrary contains 117 files (one for each element except Z = 111 and 117) with all known level schemes available from ENSDF in 2007. These files are arranged and preprocessed into an easy-to-read format for nuclear reaction codes. During preprocessing all missing spins up to the *Nmax* level were inferred uniquely for each level from spin distributions extracted from the existing data. Electromagnetic and gamma-ray decay probabilities were estimated. Missing internal conversion coefficients (ICC) were calculated using the inferred or existing spin information, in which existing multipole mixing ratios were also taken into account. Particle decay modes are also given whenever measured. In all cases, the total decay probability was normalized to unity, including particle decay channels.

The RIPL-2 and RIPL-3 DSL sublibraries have been tested in a huge number of reaction calculations using statistical model codes EMPIRE [13] and TALYS [14] as both codes use the sublibraries as the only input source of all discrete level information and transition probabilities. These routine tests

helped to disclose and correct some additional deficiencies. The reliability of the RIPL-3 version is considered to be quite high now.

AVERAGE NEUTRON RESONANCE PARAMETERS

Neutron resonance properties required as input for nuclear reaction calculations and nuclear data evaluation are neutron strength functions, average radiative widths and the average spacing of resonances. These quantities are generally obtained from the analysis of parameter sets for the resolved resonances. The experimental resolution and sensitivity limits create incomplete (missing resonances) or distorted (errors on width determination) information on the resonance parameters. Therefore, the average widths and resonance spacings cannot be directly deduced from available resonance sequences, and should always be estimated by taking into account missing resonances. Various methods for statistical analysis of missing resonances have been developed, and most of them were applied to evaluate average resonance parameters during the RIPL project.

Complete tables of average resonance parameters provided by the Beijing, Bologna and Obninsk groups were collected during the course of the RIPL-1 project [1]. All these parameters are mainly based on the analysis of the resolved resonance parameters presented in the well-known BNL compilation [15]. Despite the common base, many discrepancies were found between the average parameter estimations. These discrepancies were rather large when compared to the parameter uncertainties, especially for cases with less than 20 resonances.

After consideration of the existing discrepancies, the Beijing and Obninsk groups re-analyzed some of their previous evaluations, and prepared updated versions of the average resonance parameters. Agreement between the updated parameters has been significantly improved for most of the nuclei, although the uncertainties quoted for the Obninsk evaluations were systematicly higher than the uncertainties given in the original BNL evaluations and the revised Beijing data. Taking into account substantial differences between the uncertainties obtained by the various methods, the Obninsk evaluation of the average resonance parameters was included in RIPL-1 as the recommended file, and the Beijing evaluation as the alternative [1]. In the original BNL compilation [15], the average resonance parameters were obtained for about 230 nuclei, the Obninsk group compiled the resonance parameters for 264 nuclei [16], and the recommended RIPL-1 file included 281 nuclei [1].

All nuclei available in the alternative files of RIPL-1 but not in the recommended one were re-analyzed during the RIPL-2 stage on the basis of the updated compilation of the resolved resonance parameters. As a result, 16 nuclei were added to the list of average resonance parameters in the RIPL-2 file [2]. The corresponding average resonance parameters for the *p*-wave resonances were also added to the updated database [2].

Some skepticism can arise with respect to the recommended parameters of nuclei for which data are available for a rather small number of resonances, particularly for about 45 nuclei in RIPL-2 in which the number of resonances is equal to or less than five. Any statistical analysis of such data is doubtful. Nevertheless, it was decided to include such cases in the recommended file to provide an estimate that is certainly better than nothing.

The “Atlas of Neutron Resonances” that was published recently by Mughabghab [17] includes both an extensive list of individual resonance parameters and the updated average resonance parameters. Although for most nuclei the new average parameters were close to the old ones, the deviations exceed a double uncertainty were obtained for more than 30 nuclei.

All differences between the RIPL-2 and Mughabghab data were carefully analyzed during the RIPL-3 project. For some nuclides such differences can be related to new measurements of individual resonance parameters, which were not considered in the RIPL-2 evaluations. Another reason for the

differences is connected with a preference by Mughabghab to use the *p*-wave analysis results for the *s*-wave spacing estimation, instead of using the direct results of the *s*-wave resonance analyses.
Many discrepancies between the RIPL-2 average parameters and the Atlas evaluations [17] relate to nuclei for which data are available for less than 20 resonances. Uncertainties of obtained parameters in such cases could include beside the standard statistical uncertainties some additional systematic uncertainties which rather difficultly to estimate correctly.
All deviations between the RIPL-2 and Mughabghab estimations were re-analyzed on the basis of the individual resonance parameters included in the Atlas [17]. In the case of agreement between the reevaluated spacings and Atlas data, the last data were included in the RIPL-3 files. However, for contradictory cases the results of re-evaluated spacings were adopted.
The *s*-wave resonance spacings included in RIPL-3 are shown in Fig. 5 (left), along with the previous RIPL- 2 and Mughabghab data. Uncertainties for most of the data do not exceed the sizes of the symbols, showing that the results of all evaluations agree quite well for nuclei with more than 30 known resonances. On the whole, the data selected for RIPL-3 seem preferable for two reasons: (1) a more accurate choice of the energy interval used for the average parameter evaluations; and (2) more reliable estimation of quoted uncertainties.
The resonance spacings of the *p*-wave resonances are shown in Fig. 5 (right). These data were obtained for a smaller number of nuclei than for the *s*-wave resonances. Nevertheless, the *p*-resonance spacings data are very important in testing the consistency of the results. Based on the general statistical properties of nuclear levels, the spacings of the *s*- and *p*-wave resonances should be related by $D_1 \approx D_0/3$, at least for nuclei far from magic nuclei. This relationship is also useful for a prediction of the *s*-resonance spacing when only the *p*-resonance data are available.
Data included in RIPL-3 for the neutron strength functions are shown in Fig. 6, and compared with the RIPL-2 and Mughabghab evaluations. As a rule, there are no essential contradictions between the RIPL-3 and Mughabghab estimations. Nevertheless, it should be remarked that the RIPL-3 values were obtained from a consistent fit of the Porter-Thomas distribution of resonance widths in a carefully selected energy interval, while the Mughabghab estimations are based mainly on the analysis of widths over wide energy intervals including in some cases the unresolved resonance region.

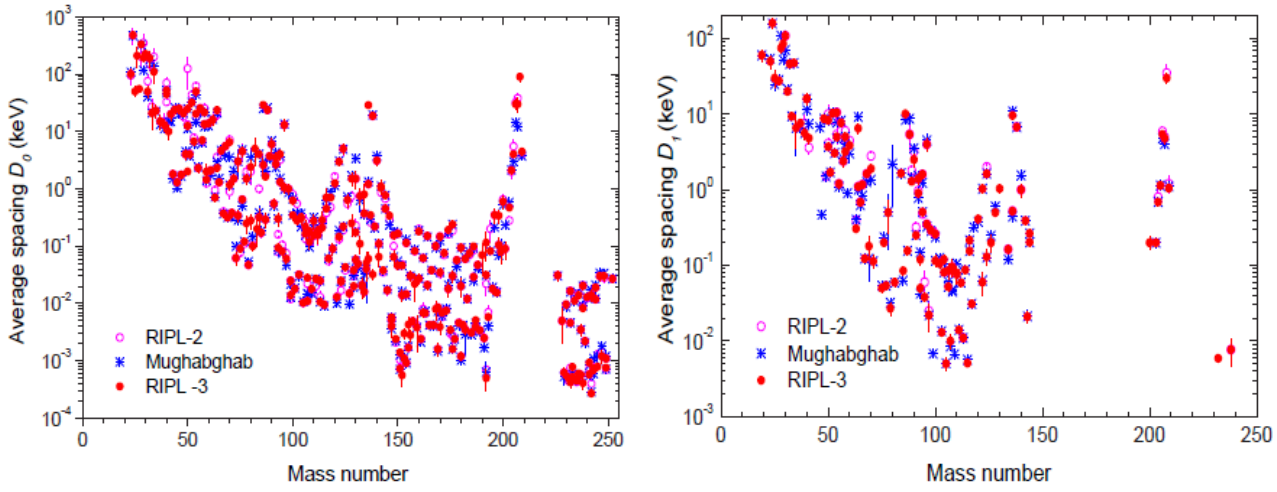

Fig. 5. Average resonance spacings for the *s*-wave (left) and *p*-wave (right) neutron resonances included in the RIPL-2 [2], Mughabghab [17], and RIPL-3 [3] evaluations.

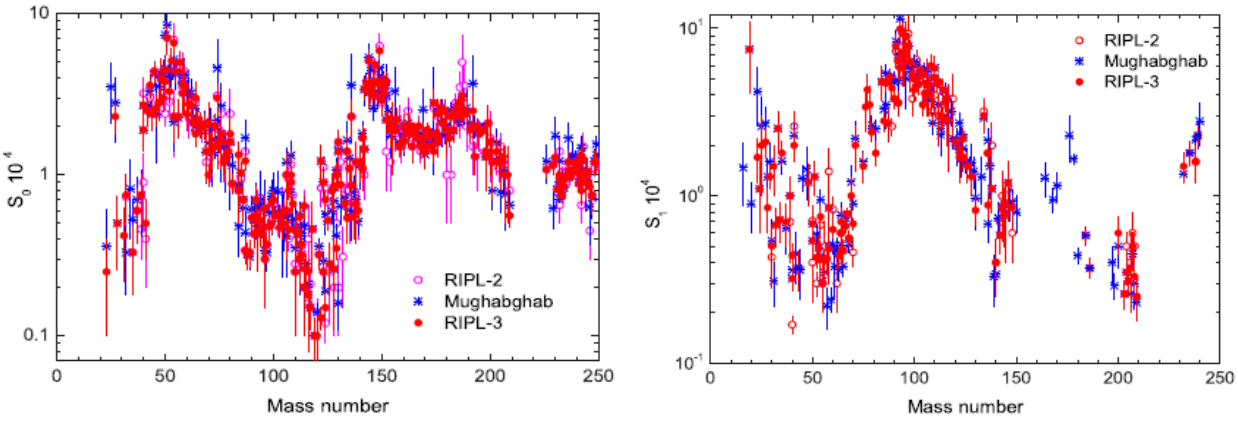

Fig. 6. The *s*-wave (left) and *p*-wave neutron (right) strength functions included in the RIPL-2 [2], RIPL-3 [3], and Mughabghab [17] evaluations.

For the average radiative widths included in the RIPL-3 files main differences relate again to the estimated uncertainties of data. For many nuclei the Atlas uncertainties [17] are smaller than uncertainties adopted in RIPL-2 and RIPL-3. However, taking into account the available width uncertainties for individual resonances, the RIPL-3 uncertainties seem more reasonable, at least for the majority of nuclei.

OPTICAL MODEL PARAMETERS

The optical model provides the basis for many theoretical analyses and evaluations of nuclear cross sections that are used in providing nuclear data for applied purposes. As well as offering a convenient tool for the calculation of reaction, elastic and (neutron) total cross sections, optical model potentials (OMPs) are widely used in quantum-mechanical pre-equilibrium and direct-reaction theory calculations, and in supplying particle transmission coefficients for Hauser-Feshbach statistical theory calculations as used in nuclear data evaluations.

The importance of optical model parameterizations is made even more apparent by the worldwide diminution of experimental facilities for low-energy nuclear physics measurements and the consequent increased reliance on theoretical methods for providing nuclear data for applications. Therefore the preservation of past work aimed at describing experimental results with optical model potentials is vital for the future development of nuclear databases. Additionally, the availability and use of microscopic optical model codes is important for predicting data for target nuclei far from the line of stability, where phenomenological models might not be valid.

The RIPL-2 OMP sublibrary was given in two parts: an archival file and a user file [2]. The archival file contained all potentials compiled so far, totaling 533, of which 287 were potentials for incident neutrons, 146 potentials for protons, 11 for deuterons, 26 for tritons, 53 for ^{3}He particles, and 10 for incident α-particles. The RIPL- 2 user file is a subset of the archival file with all single energy potentials eliminated, and contained 406 entries.

For the RIPL-3 sublibrary only the user file was included, as we have compiled only those OMPs defined in broad energy regions. There is a grand-total of 494 OMP datasets compiled into the RIPL-3 sublibrary, which comprises information published in 139 references (see the complete reference list in [3]). The RIPL-3 user sublibrary to date includes: 335 optical model parametrizations for incident neutrons, 130 parametrizations for incident protons, 13 parametrizations for incident deuterons, 2 parametrization for incident tritons, 3 parametrizations for ^{3}He particles, and 11 parametrizations for incident α-particles.

Notable additions for RIPL-3 concern dispersive OMPs and special emphasis on complex particle (deuteron and alpha) OMPs. The product of this activity for phenomenological optical potentials is an optical model potential sublibrary that contains reliable state-of-the-art parametrizations for the conventional optical model codes used in calculations of nuclear data. As well as preserving optical model parametrizations for future activities, the sublibrary offers a convenient means for evaluators to access a wide body of information on the optical model. Subroutines have been developed for reading and writing the data sublibrary and for creating convenient summaries of the sublibrary. Processing codes which permit direct interfacing of the sublibrary with the selected optical model codes – ECIS06 [18], SCAT2000 [19] and OPTMAN08 [20] – are provided.

The majority of the nucleon-nucleus potentials in the sublibrary are for single-target nuclei (or perhaps for a very narrow range of neighbouring targets/isotopes) and cover a range of incident energies. These potentials are usually the most accurate for specific targets and should be considered whenever accuracy is imperative.

There is one important series of spherical potentials which were derived as part of a comprehensive analysis covering targets from ^{24}Mg to ^{209}Bi. These are the spherical OMPs of Koning and Delaroche [21]. Other significant individual nuclide potentials include those of Arthur [22], and the extensive lists of potentials used in China [23] and Japan [24] for fission products.

The RIPL-3 OMP sublibrary contains 65 neutron and 32 proton rigid-rotor coupled-channel potentials for ground-state rotational bands. These potentials have been necessarily developed for more limited target Z and A ranges, as they depend on the structure of each target nucleus. Structure information is provided in the OMP sublibrary for the target nuclei for which the potential was determined. These potentials can be used over a broader range of target nuclei, most probably with reduced accuracy, although the user must provide the required structure information, in particular the ground-state-band deformation for rigid-rotor potentials or the dynamical deformation for the vibrational potentials. The soft-rotor potentials cannot be used for other nuclei, as the required structure information (soft-rotor Hamiltonian parameters) is difficult to extrapolate to different nuclei.

Coupled-channel potentials for incident protons are often provided for the same target nuclei as neutrons for rigid-rotor and soft-rotor potentials. These potentials were determined with neutron potentials using the Lane model [25]. The use of the term “global” refers to OMPs that cover a wide range of incident energy and target nuclei. The new important potentials, which are global for both incident neutrons and protons, are included in the RIPL-3 [4]. Their analyses have been drawn upon a wider range of experimental data than the older potentials. Particularly nice features of these depressive potentials are the reduced number of potential parameters, the energy-independent geometry and a reliable extrapolation to the low-energy region.

Uncertainties in optical model potential parameters

One of the objectives in RIPL-3 was to give an estimate of the uncertainties in the OMP parameters. This estimate was made for the Koning-Delaroche global optical model potential [21]. A Monte-Carlo method for generating uncertainties of the final cross sections and angular distributions has been used. Each nuclear model parameter is assumed to be uncertain, where the uncertainty distribution is assumed to be Gaussian. Running ECIS06 many times, where all elements of the parameter vector are *randomly* sampled from a Gaussian distribution with a specific uncertainty for each potential parameter, provides all the statistical information needed to produce a full covariance matrix. The results should be regarded as “proof of principle” only; various subtleties concerning correlation of parameters and models have been disregarded at this stage of development. It is well known that potential depths and corresponding radii are strongly correlated; therefore, the independent Monte-Carlo sampling of those parameters should be avoided. At present, we can only provide indirect proof

of the validity of the method, based on reasonable uncertainties obtained for the simulated cross sections and angular distributions.
We have adjusted the uncertainties of the model parameters (widths of the Gaussian distribution), such that we obtain reasonable agreement for a subset of the large experimental OMP database. The resulting uncertainties of the global neutron OMP parameters are listed in Table 1.
Uncertainties of geometric parameters are expected to be similar for other optical model potentials. A typical uncertainty of the real (imaginary) potential depths is estimated to be 3% (10%) below 30 MeV for other optical model potentials, reaching 5% (20%) for the real (imaginary) spin-orbit potential depths. An uncertainty of » 20% is estimated for the static deformation parameters used in coupled-channel potentials, which could be reduced to approximately 10% uncertainty if neutron strength-function experimental data are available [26].

Parameter	uncertainty (%)	Parameter	uncertainty (%)
r_V	2	d_1^n	10
a_V	2	d_2^n	10
v_1^n	2	d_3^n	10
v_2^n	3	r_{so}	10
v_3^n	3	a_{so}	10
v_4^n	5	v_{so1}^n	5
w_1^n	10	v_{so2}^n	10
w_2^n	10	w_{so1}^n	20
r_S	3	w_{so2}^n	20
a_S	4		

TABLE 1: Uncertainties of the Koning-Delaroche global neutron OMP parameters [21] (RIPL 2405), listed as fraction (%) of the absolute value.

NUCLEAR LEVEL DENSITIES

The statistical properties of excited nuclear levels have been a matter of concern and study for many years. One of the basic statistical properties of these levels is their density, for which the Fermi gas [27] and constant temperature models are frequently used with empirical input parameters obtained from fitting certain experimental data. However, the physical assumptions underlying these models are not sufficiently sophisticated to account properly for variations of level densities over a wide energy interval from the ground state to well above the neutron separation energy.
Some of the most important concepts upon which our current understanding of the structure of low-lying nuclear levels is based are shell effects, pairing correlations and collective phenomena. All these concepts have been incorporated into the generalized superfluid model developed by many authors over the last 60 years. Most consistently all these properties are taken into account in microscopic versions of the model, but phenomenological versions of the model – convenient for the analysis of experimental data – have also been developed during the previous decades.
Main relations for the nuclear level density (NLD) description were considered in the previous lecture.
All relations required for practical calculations are presented in details in Ref. [2-4]. So, we will discuss here mainly the NLD parameters recommended for different models.

Simple phenomenological models

We may distinguish between two types of phenomenological approaches depending upon whether collective effects are explicitly accounted for or not. The simplest approach: the Composite Gilbert-

Cameron Model (CGCM) and the Back-Shifted Fermi Gas Model (BSFGM) – do not take into consideration explicitly any collective enhancement of the level densities. These models are based on simple but easy to use analytical expressions with few parameters, which hopefully reduces the uncertainty of the model. On the contrary, both the Generalized Superfluid Model (GSM) and the Enhanced Generalized Superfluid Model (EGSM) explicitly deal with collective effects but at the price of introducing more complicated expressions. Different expressions for the collective enhancement are encountered in the literature, reflecting our current knowledge of such physical phenomena that is still not good enough. This fact introduces additional uncertainties in the GSM-like models. In RIPL-3, different strategies have been employed to improve the RIPL-1 and RIPL-2 systematics for all foregoing models.

To obtain the level density for the whole range of excitation energies, Gilbert and Cameron [28] proposed to combine the low-energy region (3) with the high-energy dependence predicted by the Fermi gas model. Such an approach is usually called the Composite Gilbert-Cameron model (CGCM). The regular differences of the level densities for even-even, odd and odd-odd nuclei, analogous to the even-odd differences of the nuclear masses, have been already noted in the early systematics of the experimental data. The effective excitation energy $U = E - \Delta$ is normally introduced to take this effect into account, Δ corresponds to the pairing energy that can be approximated as

$$\Delta = 12nA^{-1/2} \quad , \qquad (4)$$

where n=0, 1 and 2 for odd-odd, odd A, and even-even nuclei, respectively. The link between the parameters of the constant temperature and Fermi gas models in the CGCM can be found by imposing the continuity of the level density function and its first derivative at some matching energy U.

Analyses of the experimental data within this phenomenological approach was carried out initially in Ref. [28], and the parameters obtained by different authors in the subsequent analyses of experimental data are reported in the RIPL-1 Handbook [1]. The complete set of level density parameters obtained for the Composite Gilbert-Cameron model is given in the RIPL- 3 *density/level-density-gc.dat* file, and the format is described in the RIPL-3 *level-density-gc.readme* file [3].

Values of the level density a-parameters depend to some extent on the determination of the spin cutoff parameter. The early systematics used a value of $\langle m^2 \rangle = 0.146A^{2/3}$, which corresponds to mean-square averaging of the proton and neutron angular momenta projections over all single-particle levels occupied in the ground state of a nucleus [27]. Later analyses used different values such as $\langle m^2 \rangle = 0.24A^{2/3}$ or the rigid-body value of the moment of inertia. In the RIPL-3 analysis the spin cutoff values were calculated in accordance with the systemstics of the angular momentum distribution for low-lying levels [29]. These differences in the choice of the spin cutoff parameters, as well as some variations in the even-odd corrections to the excitation energies, should be borne in mind while comparing the a-parameters obtained by different authors.

The a-parameters derived in the RIPL-3 project are shown in Fig. 7 in comparison with the previous RIPL- 2 data. Agreement of the RIPL-3 and RIPL-2 results is reasonably good for most nuclei and the observable differences relate mainly to the updated values of the resonance spacings and to the differences in the fitting procedure.

Fig. 8 shows the matching energies E_M and the nuclear temperatures T, and the energy shifts E_0. Generally, the RIPL-3 results are close to previous RIPL-1 and RIPL-2 analyses [1, 2]. However, the matching equations for the level densities set some limitations on the temperatures and the energy shifts, resulting in differences between the values derived from the matching conditions and the same parameters estimated from the analysis of low-lying levels only. These differences can be seen in the middle plot of Fig. 8, where the temperatures obtained from the analysis of low-lying discrete levels are shown together with the temperatures derived from the level density analyses for the same nuclei.

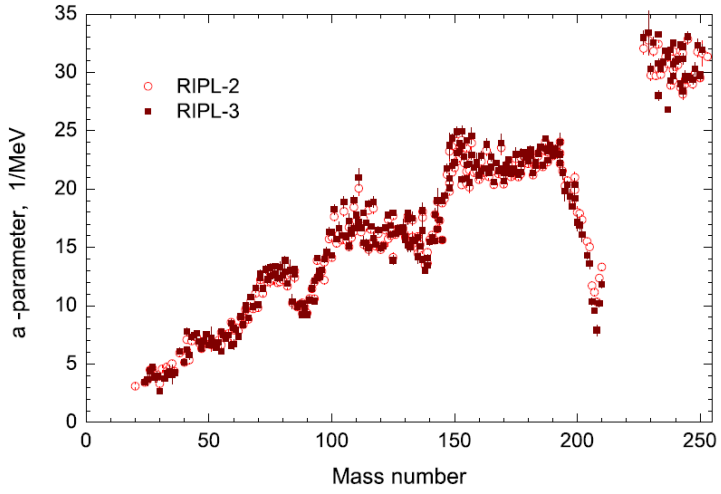

Fig. 7. Level density parameter $a(Bn)$ of the Composite Gilbert and Cameron model.

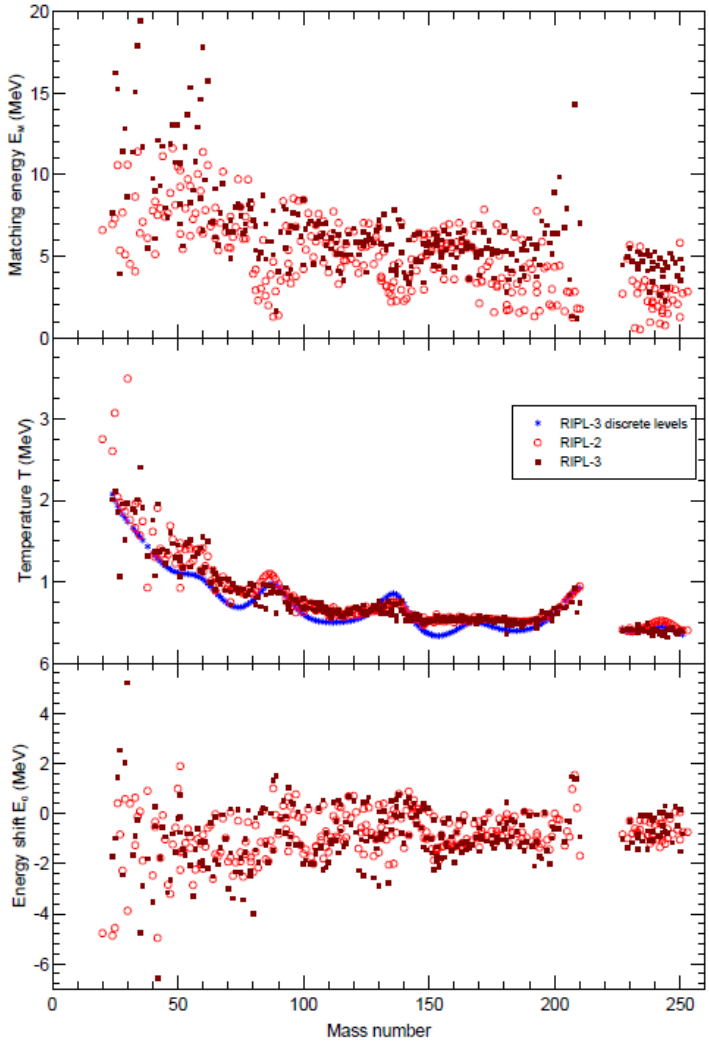

Fig. 8. Level density parameters E_M , T and E_0 for the Composite Gilbert and Cameron model.

The strong correlation of the shell corrections and the ratio $a(Bn)/A$ have always been considered as a direct evidence of the important role of shell effects in the description of level densities and other statistical characterristics of excited nuclei. On the other hand, the results of all microscopic calculations of the nuclear level densities display the damping of the shell effect at high excitation energies [30-32]. To take into account the shell effect damping, the level density parameters should be energy dependent. This dependence may be approximated by the formula [33]

$$a(U) = \tilde{a}\{1 + \delta E_0[1 - \exp(-\gamma U)]/U\}, \quad (5)$$

where δE_0 is the shell correction and $\tilde{a}$ is the asymptotic level density value obtained when all shell effects are damped. The asymptotic level density parameter may be approximated as

$$\tilde{a} = \alpha A + \beta A^{2/3} \quad , \quad (6)$$

and the damping parameter is usually selected in the form

$$\gamma = \gamma_0 A^{-1/3} \quad . \quad (7)$$

From a fit of the CGCM a-parameters (Fig. 7) with the Myers-Swiatecki shell corrections the following coefficients have been obtained (in MeV^{-1}) [3]:

$\alpha = 0.0692559$, $\beta = 0.282769$,
$\gamma_0 = 0.433090$. (8)

For nuclides with negligible or zero number of discrete levels, the empirical expression for the temperature T (in MeV) was used

$$T = -.22 + 9.4[A(1 + \gamma \cdot \delta E_0)]^{-1/2}, \quad (9)$$

that takes into account the observable shell effects (Fig. 8). The energy shift E_0 can be obtained than directly from the matching equations. In a few rare cases, Eq. (9) may lead to a matching energy E_M that is too high. In such cases the empirical expression has been

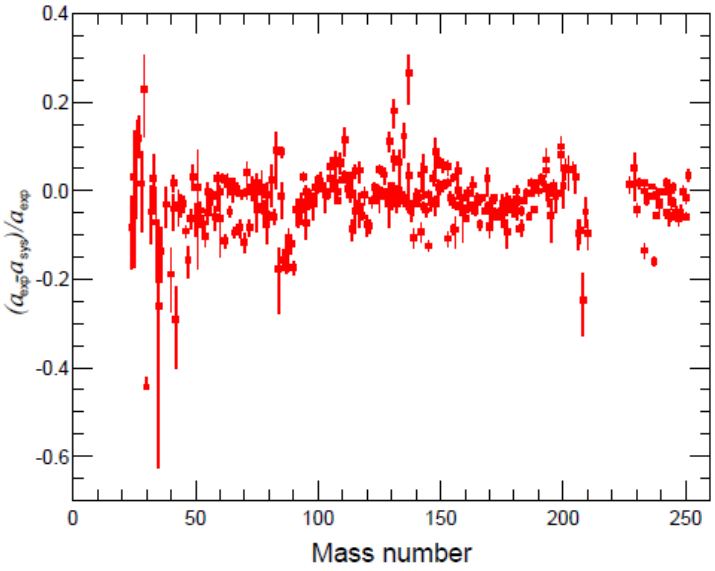

Fig. 9. Deviations between the RIPL-3 "experimental" level density parameter $a(Bn)$ derived from the CGCM resonance spacing analysis and the CGCM global systematics

applied (in MeV)

$$E_M = 2.33 + 253/A + \Delta \quad , \qquad (10)$$

and the temperature was determined then from the matching conditions.

The root mean square deviation factor $f_{\rm rms}$ can be used to estimate the overall deviation with respect to the experimental data for the neutron resonance spacings:

$$f_{rms} = \exp\Big[\ N^{-1}\sum_{i=1}^{N} \ln^2 \frac{D^i_{th}}{D^i_{\rm exp}}\ \Big]^{1/2} \qquad (11)$$

where N is the number of nuclei considered. With the above global parameters, the $f_{\rm rms}$ deviation with respect to experimental resonance spacings is $f_{\rm rms}$ = 1.76.

Deviations of the "experimental" a-parameters included in the RIPL-3 *densities/level-densities-gc.dat* file from the global a-parameters calculated on the basis of the systematics with the expressions (4)-(8) are shown in Fig. 9. Standard deviation between the "experimental" and global parameters is equal to 0.0613. This means that the systematics with global parameters describes the available a-parameters with one-sigma uncertainty of 6.1%. Similar uncertainty should be expected in evaluations of the level density parameters $a(U)$ for unknown nuclei and for the excitation energies different from the neutron binding energies.

Another approach to the problem of simultaneous description of neutron resonance densities and low-lying levels was proposed in Ref. [34]. It has been assumed that both sets of experimental data can be described on the basis of the Fermi-gas model relationships, if the level density parameter a and the excitation energy shift (4) are considered as free parameters for each nucleus. Since for odd-odd nuclei the displacement thus found is negative, the above approach has been called as BSFGM.

All data available on the neutron resonance densities and low-lying nuclear levels were analyzed, and parameters a and Δ_{eff} have been estimated for the entire mass region. Due to another determination of effective excitation energies the values obtained for the a-parameter are naturally somewhat lower then those shown in Fig. 7. However, the shell effects in the mass dependence of a-parameters remain essentially invariable. In the analysis presented in the RIPL-2 it was supposed that the level density parameter is energy independent below the neutron binding energy and Eq. (5) for the systematics of a-parameters at higher energies only. In the RIPL-3 analysis Eq. (5) was applied for the whole energy region [3, 4]. The following parameters has been for the BSFGM systematics (in MeV^{-1})

$$\alpha = 0.06926, \qquad \beta = 0.2828, \qquad \gamma_0 = 0.4331, \qquad (12)$$

and the average shift relative to Eq. (4) was equal to $0.1730 - 12A^{-1/2}$ MeV. The global parameters of BSFGM describe the experimental data on neutron resonance densities with the deviation $f$rms = 1.68. Deviations between the BSFGM "experimental" parameters $a(B_n)$ and the global systematics estimations are very close to the results obtained for CGCM (Fig. 9). It means that average uncertainty of the a-parameter systematics is practically the same for both models.

Generalized superfluid models

If collective effects are included into consideration of excited level structure [35], the nuclear level density may be expressed as:

$$\rho(E, J) = \rho_{qp}(U, J)K_{vibr}(U)K_{rot}(U), \quad (13)$$

where ρ_{qp} is the level density due to quasi-particle excitations only, and $K_{vibr}(U)$ and $K_{rot}(U)$ are the enhancement coefficients due to vibrational and rotational excitations, respectively. The relationships used for the description of the enhancement coefficients have been discussed in the previous lecture.

Quasi-particle excitations are usually described by the relations of superconductivity theory [36]. The phenomenological version of the GSM is characterized by a phase transition from the superfluid behavior at low energy [31], where pairing correlations strongly influence the level density to a high energy region that is described by the FGM. Thus, the GSM resembles the CGCM to the extent that the model distinguishes between a low energy and a high-energy region, although for the GSM this distinction follows naturally from the theory and does not depend on specific discrete levels that determine a matching energy.

The influence of pairing correlations of superconductive type on nuclear properties can be characterized by the correlation functions $\Delta_{o\tau}$, which directly determine the even-odd differences in the nuclear binding energies and the energy gap $2\Delta_{o\tau}$ in the spectrum of quasi-particle excitations of even–even nuclei. The critical temperature t_{cr} of the phase transition from a superfluid to a normal state is connected with the correlation function through the relation

$$t_c = 0.567\Delta_0 \quad . \quad (14)$$

The excitation energy corresponding to the critical temperature may be written as:

$$U_{cr} = 0.472a_{cr}\Delta_0^2 - n\Delta_0 \quad , \quad (15)$$

where n = 0, 1 and 2 for even-even, odd and odd–odd nuclei, respectively. Above the critical energy the level density and other nuclear thermodynamic functions can be described by the Fermi gas relations in which the effective excitation energy is defined as

$$U^* = U - E_{cond} \quad . \quad (16)$$

Here E_{cond} is the condensation energy that determines a reduction of the nuclear ground state energy due to the pairing correlations:

$$E_{cond} = 0.152a_{cr}\Delta_0^2 - n\Delta_0 . \quad (17)$$

To take into account the shell effects the energy dependence of the level density parameter should be modified in the corresponding way:

$$a(U, Z, A) = \begin{cases} \tilde{a}(A)\left\{1 + \delta E_0 \dfrac{f(U^*)}{U^*}\right\} \text{for U} \geq U_{cr} \\ a_{cr}(U_{cr}, Z, A) \; for \; U < U_{cr} \end{cases} \quad (18)$$

Below the phase-transition point (15) the expressions for thermodynamic functions of a nucleus are rather complex, and they will not be considered here. The complete expressions can be found in Refs. [4, 36].

To take into account possible shortcomings of the global systematics of the pairing correlation functions and collective enhancement coefficients, an additional shift of the excitation energy δ_{shift} is introduced in the GSM. The set of GSM parameters $\tilde{a}(A)$ and δ_{shift} was obtained from the simultaneous fitting of the cumulative numbers of low-lying levels and neutron resonance spacings, using the same data set as for the CGC and BSFG models. The parameters obtained under the RIPL-2 and RIPL-3

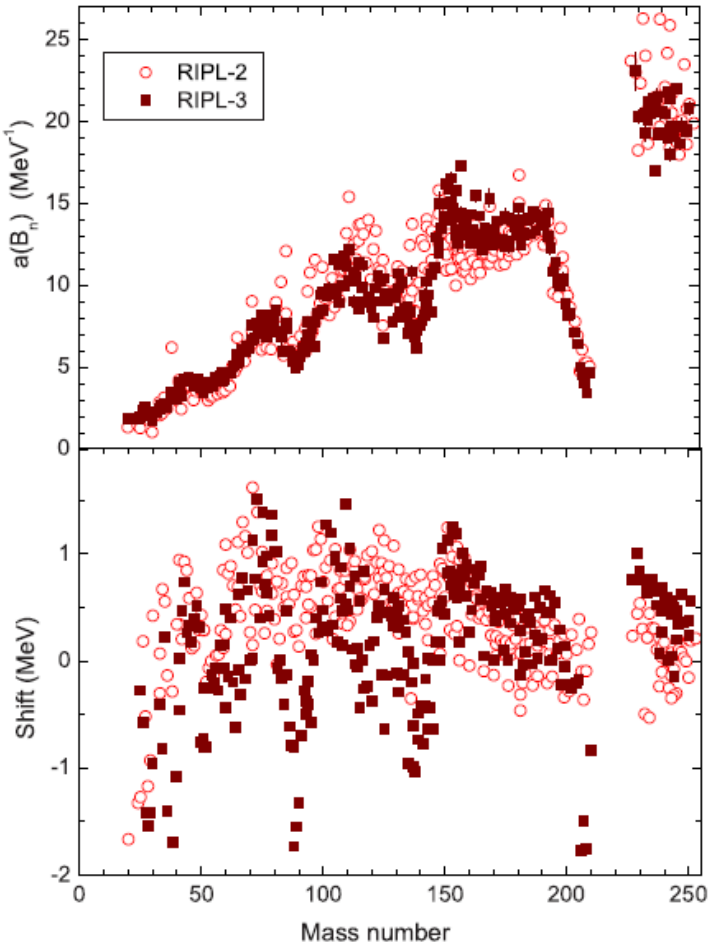

Fig. 10. Level density parameters $a(Bn)$ and $\pm shift$ for the generalized superfluid model.

projects are compared in Fig. 10 and can also be found in the corresponding *densities/level-densitiesgsfm.dat* file.

At first glance, the systematics of the level density parameters in terms of the Fermi gas and GSM models appear to be equally valid, since they give almost identical descriptions of the level densities at excitation energies close to the neutron binding energy. However, these descriptions correspond to different absolute values of the level density parameter a, because the inclusion of collective effects decreases the resulting a-parameters.

Nowadays, there is overwhelming evidence that the description of the level densities of excited nuclei should use more consistent models than those of the Fermi gas model, albeit inevitably more complex. The success of the generalized superfluid model is attributed to the inclusion of the well-known major components of nuclear theory: pairing correlations, shell effects and collective excitations. Some complexity in the model seems to be justified by the mutual consistency of the parameters obtained from the various experimental data, and by the close relationship between the theoretical concepts used to describe the structure of low-lying nuclear levels and the statistical properties of highly excited nuclei. The individual parameters are preferable for all practical applications. Parametric uncertainties are not important for prediction of the level densities in an intermediate energy region if the experimental data for neutron resonances and low-lying levels have been chosen correctly. Analyses of the evaporation spectra of different particles is of great interest in studies of the nuclear level densities. The energy dependencies of the level densities obtained from the spectrum analysis of various threshold reactions are in good agreement with the calculations based on the individual parameters of the GSM model [38].

On the other hand, many tasks require nuclear level density parameters for which no experimental data are available. Under such circumstances, global parameters may be used. Also, certain localised systematics may be proposed for these parameters that are based on extrapolations of the isotopic or isotonic changes. Experimental data on the cumulative number of low-lying levels can be fitted to one of the individual parameters, which may be advantageous in keeping the global systematics for other parameters.

We have performed the analysis to obtain global systematics of the GSM parameters. Results compared to experimental data are shown in Fig. 11. Using the Myers-Swiatecki shell corrections [11] and the collective enhancement coefficients described in Ref. [2, 3], for the asymptotic a-parameters have been obtained from a GSM least-squares fit of data the following parameters (in MeV^{-1}):

$$\alpha = 0.093 \pm 0.004, \quad \beta = 0.105 \pm 0.014, \quad \gamma_0 = 0.375 \pm 0.015, \qquad (19)$$

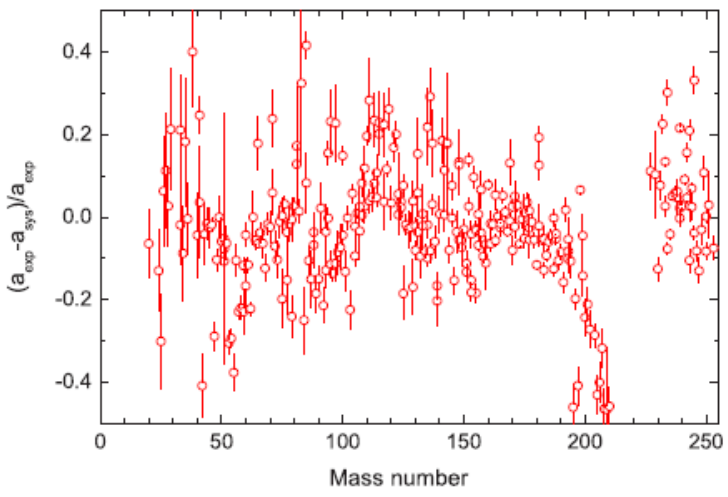

Fig.11. Deviations between the RIPL-3 "experimental" level density parameter $a(Bn)$ derived from the GSM resonance spacing analysis and GSM global systematics.

and δ_{shift} = 0.617−0.00164A MeV. Deviations between the a-parameters calculated on the basis of the above global systematics and the resonance spacing analysis are shown in Fig. 11. The standard deviation for the a-parameters is equal to 0.169 and the equivalent factor $f$rms = 1.98.

Deviations for the GSM are generally not much larger than equivalent ones for the CGCM or BSFGM. From a more careful analysis of significant deviations an impression arises that the main deviations occur for near-magic nuclei for which the shell effects are so strong that their consistent description is only possible by using microscopic models.

Deviations for the GSM are generally not much larger than equivalent ones for the CGCM or BSFGM. From a more careful analysis of significant deviations an impression arises that the main deviations occur for near-magic nuclei for which the shell effects are so strong that their consistent description is only possible by using microscopic models. Important deviations exist also for transitional nuclei in which the structure of collective excitations is intermediate between vibrational and rotational. A more accurate estimation of collective enhancements is certainly required for such nuclei to avoid the adiabatic separation of vibrational and rotational effects.

The Enhanced Generalized Superfluid Model [39] includes a more accurate treatment of high angular momenta, which are important for heavy-ion induced reactions. The properly parametrized EGSM (including adjustment to discrete levels) is the default level density formulation in the EMPIRE code [13] for calculations of nucleon induced reactions at fairly low energies; therefore, it is also referred to as "EMPIRE-specific level densities". Despite the strong link to heavy-ion physics, EGSM has been extensively used in the evaluation of low-energy neutron-induced reactions for the ENDF/BVII. 0 nuclear data library [40].

The collective enhancement compared to GSM relates to the treatment of the spin distribution in the Fermi gas model. The rotational energy in the EGSM is subtracted from the intrinsic excitation energy. This contrasts with the treatment in the models discussed earlier, in which the spin dependence is treated as a separate factor characterized by a spin cutoff parameter. The collective enhancement of the level densities arising from nuclear rotation is taken into account in the non-adiabatic form. The vibrational collective enhancement is calculated in the adiabatic approach. Vibrational energies are estimated from the liquid drop model assuming surface oscillations of the liquid drop. The formalism, inspired by the GSM, uses the superfluid model below the critical excitation energy of Eq. (15), and the Fermi gas model above. More detail consideration of the used relationships can be found in Refs. [3, 4].

The parameters α, β and γ_0 defining $\tilde{a}(A)$, and therefore the level density parameter at the binding energy $a(Bn)$, were obtained by fitting average s-wave neutron resonance spacings D_{obs} compiled in RIPL-3 with the level density formulas. The original Myers-Swiatecki shell-corrections [11], listed in the RIPL-3 *density/shellcorr-ms.dat* file, were adopted. The derived $\tilde{a}$ are shown in Fig. 11 in comparison with similar results of the GSM analysis. Differences between the a-parameters obtained are small and related to the different parametrization of the vibrational enhancement of

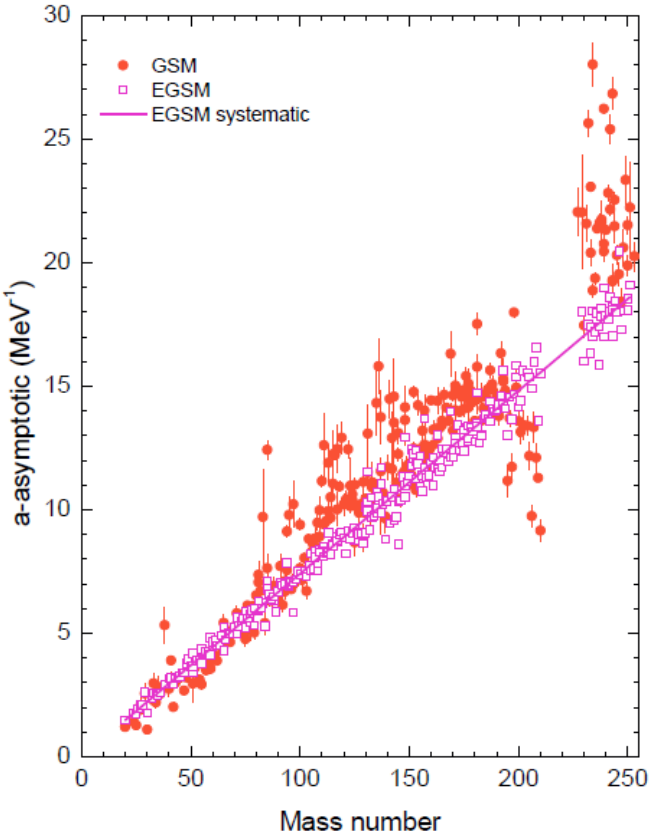

Fig. 11. Mass dependence of the asymptotic level density parameter ˜*a* for the EGSM vs the GSM results. The EGSM values were obtained by normalizing the localized EGSM systematics to reproduce each experimental *a*(*Bn*).

the level densities. The resulting global EGSM systematics is represented by the following set of parameters (in MeV^{-1}):

$\alpha = 0.0741, \quad \beta = 0.0003, \quad \gamma_0 = 0.5725.$ (20)

These parameters yield $f_{\rm rms} = 1.70$.

Contrary to other level density models considered in RIPL-3, the EGSM global systematics does not account for discrete levels. Instead, the adjustment is performed automatically by the EGSM code (provided in RIPL-3) when level densities are calculated. A shift is applied to the excitation energy to reproduce the cumulative number of levels at the energy corresponding to the highest level considered in the calculations. This shift is linearly decreased with increasing energy in such a way as to reach zero at the neutron binding energy. Therefore, adjustment to discrete levels never changes level densities at and above the neutron binding energy, ensuring that the global EGSM systematics parameters are independent of the number of adopted discrete levels. We stress, however, that level densities below the neutron binding energy strongly depend on the selection of discrete levels; thus the user is advised to inspect carefully the cumulative plots generated by the EGSM code to ensure that a proper number of discrete levels is included in the calculations.

Values of the level density parameter at neutron binding energy *a*(*Bn*) are compared against experimental data in Fig. 12 (left panel). The systematics describes adequately the shell structure, but tends to underestimate scatter of the experimental points for the deformed nuclei, especially for the actinides.

It has been observed that *a*(*Bn*) for a given element reveals rather smooth dependence on the neutron number. These shapes for individual elements are usually quite well approximated by the global systematics while the absolute values are predicted with lesser accuracy. The global systematics can be improved by applying normalization factors defined for each element for which experimental *a*(*Bn*) are available. The localized level-density systematics obtained for EGSM is given in the *densities/leveldensities- egsm-norm.dat* file. Results obtained with such localized EGSM systematics are plotted in Fig. 12 (right panel) showing an improvement in comparison with the global one, especially for actinides ($N > 126$), and near the extremes of the distribution at neutron numbers $N \approx$ 50, 64, 82 and 94–110. The localized systematics accounts for an unknown *Z*-dependence that is either not considered in the shell corrections or included improperly. This improvement comes at the cost of an additional 83 parameters, but maximizes experimental input in estimating level densities for nuclei for which experimental resonance spacings are not available.

Microscopic total level densities

Most semi-empirical approaches to level densities such as those described in the previous section are

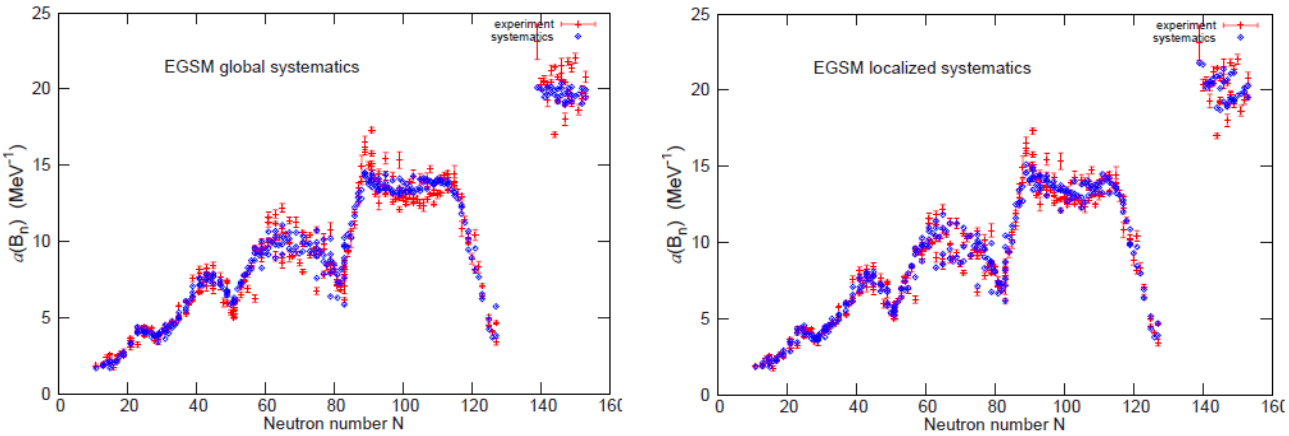

Fig. 12. Level density parameter $a(Bn)$ at the neutron binding energy. Left panel: Predictions of the global EGSM systematics (blue squares) are compared with the experimental data (red points with error bars). Right panel: Predictions of the localized EGSM systematics (blue squares) are compared with the experimental data.

based on various simplifying approximations. Such approaches often account inadequately for shell effects, pairing effects and parity distributions. More involved microscopic methods have been developed to address these deficiencies and calculate realistic level densities using the single-particle level scheme of the shell model, taking into account both short-range (pairing) and long-range (collective) interactions.

During the RIPL project we studied several microscopic methods for level density calculations. The Microscopic Superfluid Model used the same physical approaches as the considered above generalized superfluid model, but all calculations of the level density and other statistical characteristic of excited nuclei are performed on the basis of the realistic single-particle level schemes [30, 31]. The codes required for such calculations are included in the RIPL-1 and RIPL-2 libraries. Collective effects are taken into account in these codes using the same approximations as for the discussed above GSM. The single-particle level schemes of Moeller *et al.* [6] are recommended for such calculations because they were also used to determine the recommended nuclear binding energies, shell corrections and deformations. Therefore, their application to the level densities provides the desired consistency between the ground and excited states.

An alternative description of nuclear level densities has been proposed in Ref. [29], based on the extended-Thomas-Fermi plus Strutinsky-integral model for the ground-state properties, the single-particle level schemes and pairing strengths. These level schemes have been used to produce level density tables for nearly 8000 nuclei [2]. Although this approach reproduces reasonably the experimental neutron resonance spacings for many nuclei, some large deviations have been found (for example, in the Sn region). Additionally, the traditional statistical approximations used in calculations cannot describe typical fluctuations of the level density observed at low energies.

Some of those deficiencies have been removed in the HFBCS-based model [41], which predicts all the experimental resonance spacings with a accuracy comparable to the equivalent data obtained by the phenomenological RIPL-2 BSFGM formulas ($f$rms = 2.14 for the ratios D_{th}/D_{exp}). This model is based on the HFBCS ground-state description [41] with a nucleon effective mass close to the real mass, a property of particular importance for level density evaluations that provides a reasonable description of the single-particle level density near the Fermi surface. HFBCS quantities relevant to the level density calculations can be found in the RIPL-2 web site (*densities/singleparticle-levels/spl-hfbcs/* directory), including the deformation parameters, the single-particle level schemes, pairing strengths and the corresponding cut-off energies for both the neutron and proton. These schemes have been used to provide the tables of the spin-dependent level densities within the statistical approaches.

The above microscopic approaches are limited at low excitation energies, where the standard saddle-point method breaks down and non-statistical fluctuations of level densities are known to be significant. A combinatorial method can provide NLDs as a function of the excitation energy, spin and parity without any *a-priori* assumption on the spin and parity distributions of levels. Various combinatorial approaches involving exhaustive counting of particle-hole configurations have been proposed [42-45], however, they were mainly focused on the level density of intrinsic excitations.

A microscopic combinatorial approach was developed during the RIPL-3 stage to include in the level density calculations both collective effects and all possible particle-hole excitation with an improved treatment of the pairing interaction [46]. This method consists of using single-particle level schemes obtained from the constrained axially symmetric Hartree-Fock-Bogoliubov (HFB) method based on the BSk14 effective Skyrme force [8] to construct incoherent particle-hole state densities $\omega_{ph}(U,M,\pi)$ as functions of the excitation energy U, the spin projection M on the intrinsic symmetry axis, and the parity π. It is worth mentioning that this HFB+BSk14 method is also used to provide the microscopic masses, the fission barriers and fission level densities in the whole RIPL-3 project, thus ensuring a global coherence for the microscopic ingredients employed for nuclear reaction calculations.

Once all particle-hole state densities are determined, we must account for collective effects. The choice of multiplying the level densities by the phenomenological vibrational enhancement factor was made in Ref. [46], after accounting for rotational motion, if necessary (i.e. for deformed nuclei). The resulting NLDs were found to reproduce rather well the available experimental data.

To improve the phenomenological treatment of vibrational effects the boson partition function was added to combinatorial calculations [47]. The quadrupole, octupole, and hexadecapole collective excitations were taken into consideration. Simple phenomenological expressions have been proposed to estimate the energies of such excitations for all nuclei. The calculated vibrational state densities were than folded with the incoherent particle-hole state densities to obtain the total state density. The level density can be calculated from the state densities by the standard method [27].

It is well known that the introduction of the boson partition function to calculate the vibrational state density has an important disadvantage: because of violation of the Pauli principle, spurious states occur among the multiphonon excitations, and their number rapidly increases with the number of excited spacing. phonons. Moreover, for multiphonon states it is necessary to take into account the changes in phonon structure due to the weakening of the pair correlations, and the increasing admixture of particle-hole states eventually leading to the damping of the collective motion. Rigorous consideration of all these effects is an extremely complex problem, to which no satisfactory solution has yet been found.

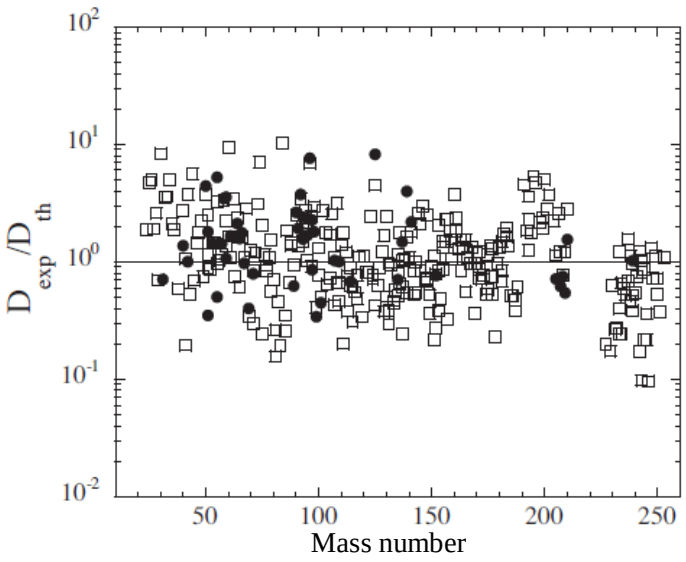

Fig. 13. Ratio of the HFB combinatorial (*Dth*) to the experimental (*Dexp*) *s*-wave (open squares) and *p*-wave (full circles) neutron resonance spacings compiled in RIPL-2.

An empirical solution is to restrict the number of phonons that can be coupled to one another. Several tests have been performed to optimize the reproduction of experimental data on the neutron resonance A maximum number of three coupled phonons folded in with particle-hole configurations with a total number of particles lower than or equal to three results in a fairly good reproduction of $D_0(B_n)$, as shown in Fig. 13. Of course,

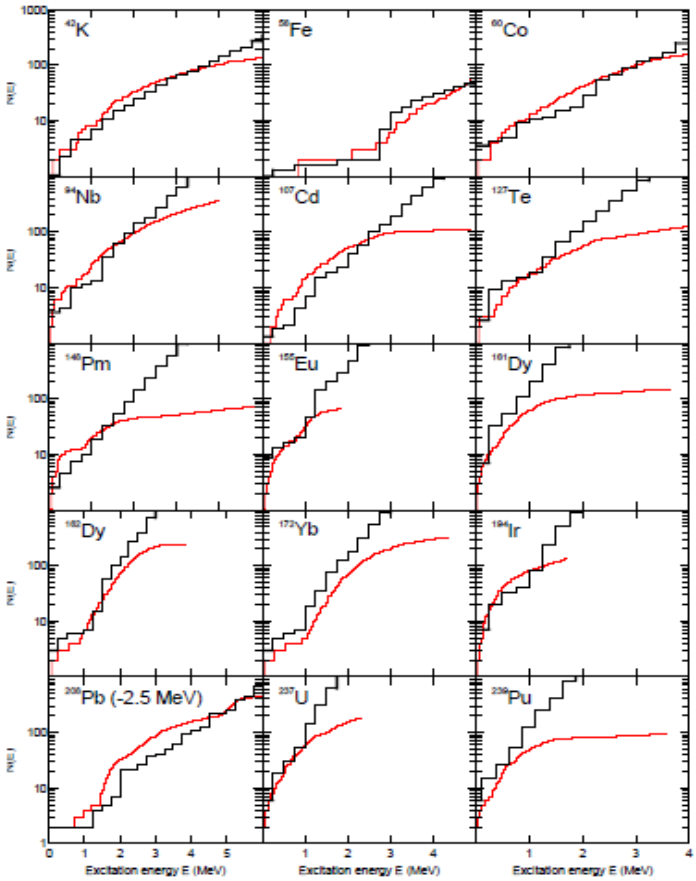

Fig. 14. Comparison of the cumulative number of observed levels (thin red staircase) with the HFB combinatorial predictions (thick black lines) as a function of the excitation energy for some nuclei. For 208Pb, both curves have been shifted by 2.5 MeV.

it has to be noted that the chosen maximum number of phonons, and the corresponding cutoff in the number of folded intrinsic configurations is arbitrary. This is certainly a weakness of the method that needs improvement. Further investigations of the vibrational enhancement and its damping are certainly needed.

Globally, the D_0 values are predicted within a factor of two. The value of the factor $f_{\rm rms}$ given by Eq. (11) found with the present approach is equal to 2.3 including both the *s*- and *p*-wave resonance spacing data. This result is to be compared to the *f*rms = 1.98 deviation of the global generalized superfluid model, or with the *f*rms = 1.70 deviation of the global EGSM. Therefore, the present approach gives only slightly worse predictions with respect to the other consistent global models.

The HFB combinatorial model also gives satisfactory extrapolations to low energies. As an example, the predicted cumulative number of levels $N(U)$ are compared in Fig. 14 with the experimental data on low-lying levels for 15 nuclei including light as well as heavy species, and spherical as well as deformed species.

The level density overestimations for deformed nuclei seen in Fig. 13 at low energies (rare-earth and actinide nuclei) are a direct consequence of using the rigid-body moment of inertia in calculations of the rotational enhancement of the level density. The experimental values of the moment of inertia for low-lying rotational bands correspond to about three times lower values. So, a more accurate approxi-mation of the moments of inertia could substantially improve the description of the experimental data for low-lying levels by means the HFB combinatorial model.

For the phenomenological models, the fit to the available experimental data was made by the adjustment of several model parameters. Similar fits can be achieved with the microscopic level densities, if the tables provided are renormalized using the scaling function

$$\rho(E,J,\pi) = \exp(c\sqrt{E-p})\rho_{HFB}(E,J,\pi) \qquad (21)$$

where ρ_{HFB} is the original HFB level density. The shift p corresponds simply retrieving the level density from the table at a different energy, while the constant c plays a role similar to that of the level density parameter a of phenomenological models. Adjusting p and c together gives flexibility at both low and higher energies, so that both the discrete levels and the experimental resonance spacings can be reproduced as well as possible. For nuclei with unknown resonance spacings, c is set to 0 and p is the only parameter enabling a fit to the discrete levels.

The microscopic model has been renormalized to experimental data (nearly 300 neutron resonance spacings and 1200 low-lying level schemes) to account for the available experimental information and can consequently be used for practical applications. The normalization *c* and *p* parameters are listed in corresponding *zXXX.cor* files. The HFB combinatorial level density tables are provided in the RIPL-3 directory *densities/level-densities-hfb*, and are not normalized. The data provided in table format for about 8000 nuclei with $8 < Z < 110$ lying between the proton and the neutron drip lines. Each table includes the spin-dependent level densities at energies up to $U = 200$ MeV and spin up to J=29 (59/2) for each isotope considered. The nuclear temperature, cumulative number of levels and total level and state densities are also included in these tables. Such structure offers a possibility to modify the HFB level density by means the normalization parameters *c* and *p*, as is usually done with analytical level-density parameters to fit some experimental data.

Partial level densities

The partial level density is used in pre-equilibrium reaction calculations to describe the statistical properties of particle-hole excitations [48]. Since the pioneering studies by Strutinsky [49] and Ericson [50] numerous theoretical methods have been developed to determine partial level densities (PLD), and a variety of approaches have been used in pre-equilibrium calculations. Some of these studies involve theoretical methods for incorporating physical phenomena such as shell effects and residual pairing interactions [51-53].

The most widely used approach to PLD is an equidistant single-particle model using closed-form expressions, as proposed by Williams [54], and further refined by many authors. Despite extensive research, even the most sophisticated theoretical predictions can significantly deviate from reality. Difficulties arise in testing the validity of determining partial densities through comparison of calculated and measured pre-equilibrium spectra because of the uncertainties in our understanding of the pre-equilibrium reaction mechanisms. Moreover the partial level density is not a directly measurable quantity. State-of-the-art methods to calculate PLD were reviewed by Betak and Hodgson [55].

RIPL-2 [2] includes a code written by M. Avrigeanu and V. Avrigeanu to calculate partial level densities using various models as described in their extensive paper [56]. During the RIPL-3 projects some attempts have been made to calculate particle-hole level densities using the combinatorial HFB+BSk14 method [47]. However, the resulting partial level densities have not been validated in pre-equilibrium model calculations, as the use of particle-hole level densities containing collective effects in current pre-equilibrium models is not straightforward.

The closed-form expression for PLD derived in the equidistant spacing model [55, 56] is adequate for many pre-equilibrium calculations, and easier to implement than many other more complex recommendations [2].

GAMMA-RAY STRENGTH FUNCTIONS

Gamma emission is an important channel for nuclear de-excitation accompanying the final stages of almost all nuclear reactions.

The gamma-decay strength function is defined as the ratio of the average reduced radiation width to the average level spacing:

$$\vec{f}_{Xl}(\varepsilon_\gamma) = \left\langle \Gamma_{XL}(\varepsilon_\gamma) \right\rangle / \varepsilon_\gamma^{2l+1} D_l \quad . \qquad (22)$$

where ε_γ is the gamma-ray energy and the *X*-index corresponds to the electric *El* or the magnetic *Ml* transitions of *l*-multipolarity. The dominative ones are the *E1*, *M1* and *E2* gamma-transitions. In a similar way the gamma-absorption strength function can be determined that is connected with the photo-absorption cross section by the relation

$$\vec{f}_{Xl}(\varepsilon_\gamma) = \left\langle \sigma_{XL}(\varepsilon_\gamma) \right\rangle / (2l+1)(\pi\hbar c)^2 \varepsilon_\gamma^{2l-1} \quad . \tag{23}$$

Experimental gamma-ray strength functions

Experimental gamma-ray strength functions have been collected over a period of about sixty years, based on measurements of partial radiative widths by three different types of experiment. Most of the data are derived from discrete resonance-capture measurements using the method of slow neutron time-of-flight spectrometry to determine the incident neutron energy. Gamma-ray spectra following the thermal neutron capture are used also with some restrictions to derive the gamma-ray strength functions. Another source of data is provided by photonuclear reactions. Analysis of all these experiments involves averaging over Porter-Thomas fluctuations, which governs the distribution of partial radiative widths.

The most extensive compilation of experimental gamma-ray strength functions for the fixed gamma-ray and excitation energies was presented in RIPL-1 [1]. These data were also adopted for RIPL-3. E1 and M1 strength functions are given for nuclei from ^{20}F up to ^{239}U, and some of the original results were corrected on new reference data and nonstatistical effects.

Some important data on the dipole radiative strengths at the energies from 6 to 10 MeV were obtained by studying the gamma-ray spectra in the charged particle-induced reactions [57, 58]. The precision data on the low-energy behaviour of strength functions have recently obtained also in the photon scattering experiments [59 - 62].

Closed-form models for the E1 strength function

The absorption and emission of dipole gamma-rays in the energy region up to 30 MeV is mainly governed by excitation of the giant isovector dipole resonance (GDR). At energies around the GDR, the photo-absorption cross sections for medium and heavy nuclei are well approximated by the Lorentzian function and in accordance with the Brink hypothesis the same function can be used to describe the gamma-decay strength functions

$$\overleftarrow{f}_{E1}(\varepsilon_\gamma) = \vec{f}_{E1}(\varepsilon_\gamma) = 8.674 \cdot 10^{-8} \frac{\varepsilon_\gamma \sigma_r \Gamma_r^2}{(\varepsilon_\gamma^2 - E_r^2)^2 + \varepsilon_\gamma^2} \text{ MeV}^{-3}, \tag{24}$$

where the Lorentzian parameters σ_r, E_r, Γ_r are the peak cross section, the GDR energy and the resonance width, respectively; the energies and widths are given in units of MeV, and σ_r in mb. The E1 strength functions in deformed nuclei are taken as the sum of two Lorenzians, each with the corresponding energy, width and peak value for the photo-absorption cross section.

Eq. (5) with a constant value for the GDR width is usually named the Stanard Lorenzian model (SLO) and the RIPL-3 contents the complete set of model parameters estimated from the observed photo-absorption cross sections [1]. Unknown GDR parameters can be estimated from the phenomenological systematics based on some theoretical models and the corresponding interpolation of experimental data. The simplest systematics for spherical nuclei is the following:

$$E_r = 27.47 A^{-1/3} + 22.06 A^{-1/6} \text{ MeV}, \tag{25}$$

$$\Gamma_r = 2.77 \cdot 10^{-6} E_r^{1.9} \text{ MeV}, \qquad S_r = \tfrac{\pi}{2} \sigma_r \Gamma_r = 76 NZ / A \text{ mb MeV},$$

where S_r is the total energy integrated cross section for electric-dipole photon absorption. For deform nuclei the GDR splitting should be taken into account [1].

Generally, the SLO model with adjusted parameters looks the best approximation of the gamma-ray strength functions for energies above the neutron binding energy, but for lower energies this model overestimates in many cases the available experimental data especially for the near magic nuclei [63 – 65]. To improve a description of experimental data the Modified Lorenzian models (MLO) have been proposed which include some additional energy and temperature dependences of the GDR widths. In

some model versions, particularly, in the Enhanced Generalized Lorentzian model (EGLO) a nonresonance component was added to the Lorentzian function [64]. More detail discussion of various versions can be found in Ref. [4].

Two typical examples of experimental data descriptions by different models are shown in Figs. 15 and 16. It is obviously that the MLO models are preferable for a description of the low-energy behavior of the gamma-ray strength function. However, a limited amount of experimental data does not allow yet to select the best MLO model and to verify a uniform application of model parameters for all medium and heavy nuclei.

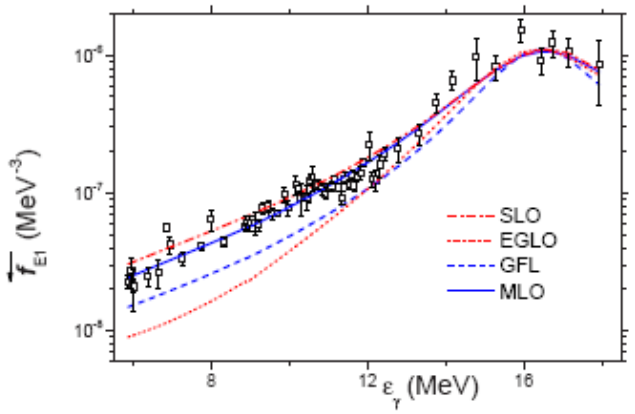

FIG. 15. E1 gamma-ray strength function plotted against energy for ^{90}Zr; experimental data are taken from Ref. [66].

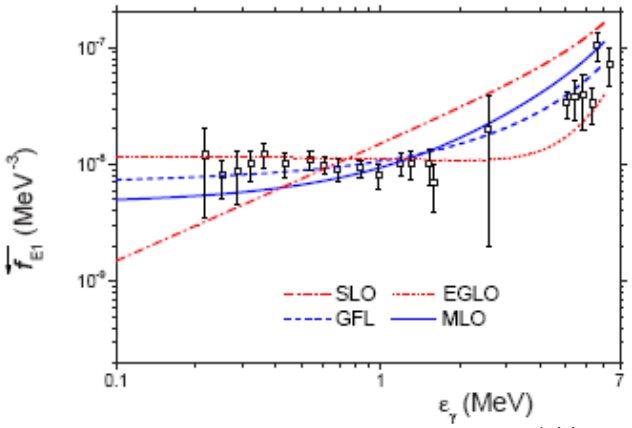

FIG. 16. E1 gamma-ray strength function of ^{144}Nd for *Ui* = *Bn*:experimental data are taken from Ref. [67].

Microscopic approach to E1 strength function

Many microscopic models have been developed with the aims of providing predictive power and reasonably reliable E1 strength functions. Attempts in this direction have been specifically conducted within the quasi-particle random-phase-approximation (QRPA). The Hartree-Fock-Bogoliubov model (HFB) including the realistic Skyrme interaction plus QRPA approach has been used for large-scale derivations of the E1 strength function [68]. The final E1 strength functions obtained by folding the density of QRPA excitations for a given spin and parity (QRPA strength) with a Lorentzian function also reproduce photoabsorption satisfactorily, as well as the average resonance capture data at low energies [68]. QRPA distributions in the neutron-deficient region and along the valley of β-stability are very close to a Lorentzian profile in the MLO model.

Significant departures from the Lorentzian shape are found for nuclei with a large neutron excess. QRPA calculations [69 - 71] show that neutron excess affects the spreading of the isovector dipole strength, as well as the centroid of the strength function. The energy shift is found to be larger than predicted by means of the usual dependence (25) given by the phenomenological models. Some extra strength that increases with neutron excess is also predicted to exist at sub-GDR energies. Even if this behaviour represents only a few percent of the total E1 strength, an increase by up to an order of magnitude of the radiative capture cross section can occur for some exotic neutron-rich nuclei [68].

RIPL-3 provides improved predictions of the GDR energies and widths for about 6000 nuclei from 14 $<Z<$110 between the proton and the neutron drip lines. Comparisons between predicted and experimental GDR energies and widths are shown in Fig. 17 for the RIPL-3 experimental compilation; more details can be found in Ref. [72]. It can be seen that some systematic differences exist between the theoretical calculations and experimental data especially for the width values. It is necessary also to note that uncertainties of the experimental data for widths are rather large for many nuclei.

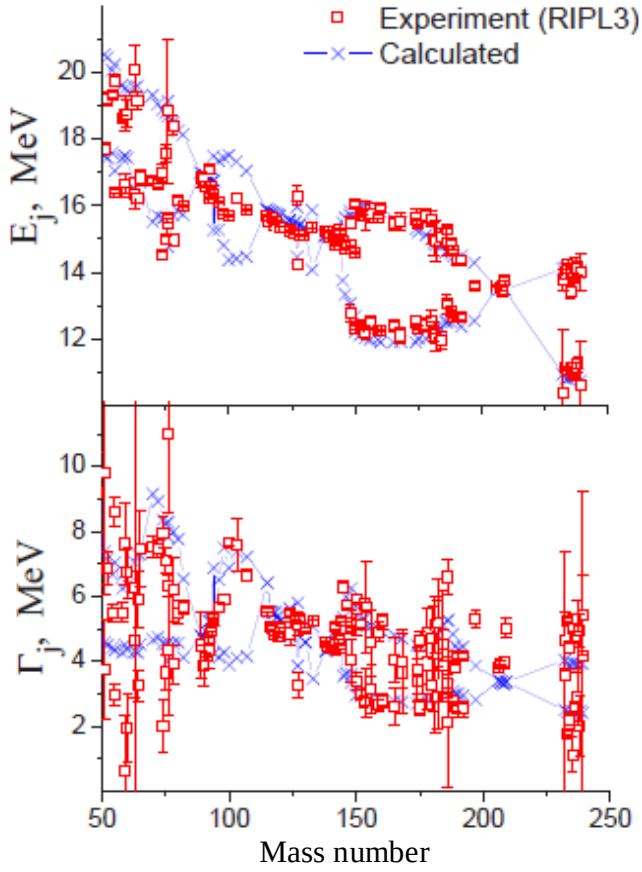

FIG. 17: Comparison of experimental data with the calculated GDR energies and widths given in the *gamma/gdr-parameters-theor.dat* file.

M1 and E2 transitions

The giant resonance with the energy of 8...9 MeV and the width about 4 MeV has been observed for the gamma-ray strength functions of the dipole magnetic transitions [73]. At energies close to the neutron binding energy the available experimental data on the dipole magnetic transitions corresponds to an average value of the M1 strength functions [63]

$$f_{M1} = (1.6 \pm 0.4) \cdot 10^{-8} \quad \text{MeV}^{-3} \quad .$$

There is a considerable dispersion of the data relative to the averaged value. Errors of strength function evaluations are also big for many nuclei because of a limited number of neutron resonances used for the strength function analysis.

The available resonance data [63] on the E2 strength functions can be approximated by the relation

$$f_{E2} = (1...3) \cdot 10^{-14} \cdot A^{4/3} \quad \text{MeV}^{-5}$$

E2 radiation is linked to the excitation of the giant quadrupole isoscalar resonance, the Lorenzian parameters of which can be estimated nowadays only with large uncertainties.

An overall comparison of the calculations and experimental data shows that the MLO approaches with asymmetric Lorenzian function provide a reasonably method of estimating the gamma-ray strength functions over a wide energy range. However, more precise experimental data are needed to improve the determination of the temperature and energy dependence of the strength functions, so that the contributions of the different mechanisms responsible for the damping of the collective states can be further investigated. Such data could help also to discriminate between the various closed-form MLO models and to improve the folding approximations used in the microscopic models.

NUCLEAR FISSION

Nuclear fission remains the most complex topic in applied nuclear physics. Since its discovery, nuclear fission has always been an active field of research both as a purely theoretical challenge, as well as for practical applications.

The RIPL project had no intention to cover the whole complexity of fission phenomena. Instead we focus on the input parameters needed in fission cross-section calculations for energy and non-energy applications. The most important of these activities are the following:

• The broad scale investigations of the fission cross sections for pre-actinides that undergo different charged-particle induced reactions provide the main experimental information on the droplet properties of nuclei. The interest in such data has increased dramatically over the previous decade due to extensive discussions of accelerator-driven power systems for the transmutation of nuclear waste.

• The highly accurate studies of actinides that undergo neutron-induced reactions have a significant importance in reactor physics. Such studies are extended to the high energies of neutron and charged-particle induced reactions to address the needs of emerging nuclear technologies such as accelerator-driven systems or production of alpha emitters for radiotherapy. They also allow the investigation of the changes of fission barriers with increasing excitation energy.
• Microscopic calculations of fission barriers are required to explain the existence of long-lived superheavy elements with $Z > 102$ and to provide extensive data on fission for astrophysics, which encompasses stellar nucleosynthesis and the rapid neutron capture process.

Fission input data for pre-actinides

Interest in the fission data for pre-actinides has increased dramatically over the previous decade, especially due to the programs related to accelerator-driven power systems for the transmutation of nuclear waste. Therefore, a special section in RIPL-2 was dedicated to this subject [2].
As far as light pre-actinide nuclei are concerned, most measurements of the fission cross sections were performed at energies above the fission barriers. The fission width for such energies can be written in the form

$$\Gamma_f(U) = \frac{1}{2\pi\rho_c(U)} \int_0^{U-B_f} \rho_f(U - B_f - E)dE \quad , \qquad (28)$$

where ρ_c and ρ_f are the level densities for the compound and saddle configurations, respectively, and B_f is the fission barrier height. Eq. (28) shows the strong interdependence of the barrier parameters and the level densities.
A large amount of data on the fission barriers has been accumulated from light charged-particle-induced reactions [74 - 77]. These data were provided in the *fission/fission-barriers-exp.dat* file in RIPL-2 together with the experimental fission barriers for actinides. Many measurements of fission cross sections were also performed through heavy-ion induced reactions [78]. However, because of the rather complex models involved in the analysis of heavy-ion reactions, the uncertainties in the estimated fission barriers are usually found to be much larger than for light charged-particle reactions.
Generally, fission barriers for pre-actinides are approximated by the equation:

$$B_f = B_{LD} - \delta E_0 + \delta E_f \quad , \qquad (29)$$

where B_{LD} is the liquid-drop component of the fission barrier, δE_0 is the ground-state shell correction, and δE_f is the corresponding shell correction for the saddle-point configuration. Usually, one assumes that the shell effects vanish for the strongly deformed saddle configurations of pre-actinides (i.e., δE_f =0), and the ground-state shell corrections are equal to the microscopic corrections in the nuclear masses. Differences between the various estimates of the fission barriers relate mainly to the liquid-drop component of the fission barrier.
Available experimental data on the fission barriers for pre-actinides are compared in Fig. 18 with the simple barrier description proposed by Mayer-Swiatecki [79]. The FRDM shell corrections were used to transform the experimental fission barriers to liquid-drop barriers. The good description of the experimental barriers allows recommending the Mayer-Swiatecki approach as probably the best approximation of liquid-drop fission barriers in the region of $Z^2/A > 30$. Lighter nuclei have a dumb-bell shape at the saddle point, and the calculations based on the Yukawa plus- exponential double-folded approximation for nuclear energies may be preferable [80]; therefore, for nuclei with $Z < 80$ the liquid drop barriers described by Sierk's code [80] *fission/fis-barrier-liquiddrop.for* (provided in RIPL-2) are recommended with the addition of the ground-state shell corrections estimated by the Myers-Swiatecki mass formula [11].

All level-density models considered above can be used to calculate the fission widths. Statistical calculations are very sensitive to the level-density ratio. Therefore, it is desirable to use the same level-density model to calculate the fission and particle widths. For the same reason, it is also recommended to use the same level-density formalism for the ground-state and saddle-point deformations. However, the shell, pairing and collective effects are essentially different for the ground and saddle-point states, and these differences should certainly be taken into account in calculations of fission cross sections. Shell effects can apparently be neglected for the saddle level densities, but they are important for the neutron widths of near-magic nuclei shown in Fig. 18. The energy dependence of the *a*-parameter is extremely important for such nuclei, as confirmed by many results of fission cross-section analyses [81, 82].

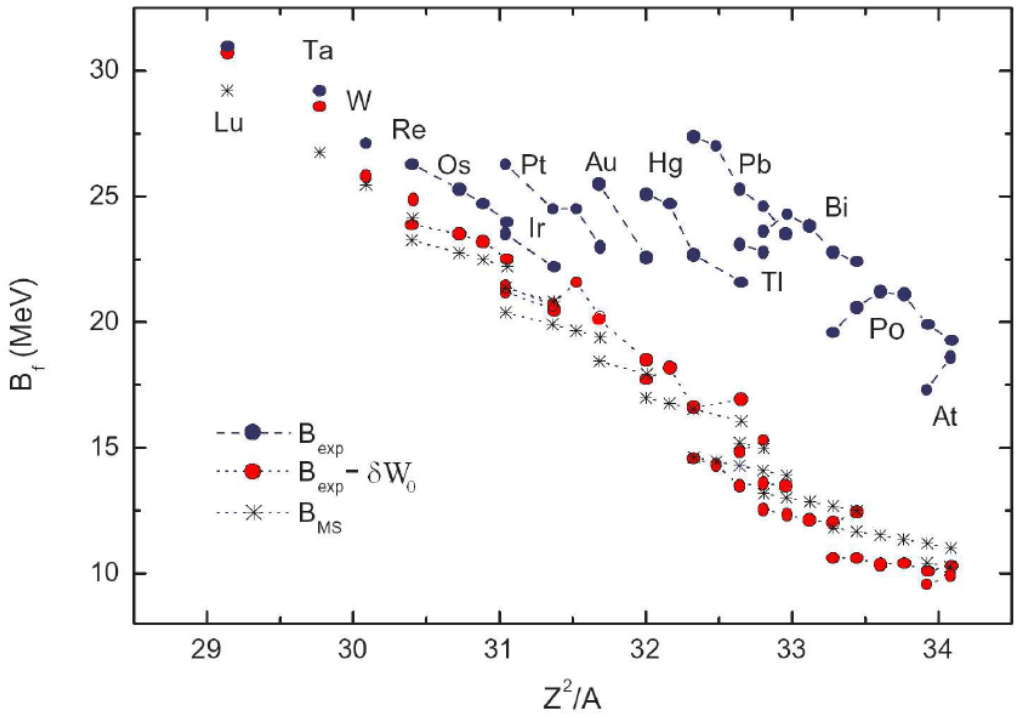

FIG. 18: Experimental fission barriers of pre-actinides and their liquid-drop components in comparison with LDM estimates [79]

Pairing effects are implicitly associated with the energy dependence of the effective moment of inertia, which determines the angular distributions of the fission fragments [83]. Analysis of the corresponding experimental data has shown that the correlation parameter for the saddle point Δ_f should always be specified as about 15% larger than for the ground state [84]. The relationship $\Delta_f = 14A^{-1/2}$ MeV can be used as a reasonable approximation for the pairing parameter at saddle points. Collective enhancement of nuclear level densities is clearly displayed in a systematic analysis of the fission cross sections for spherical and deformed nuclei [85, 86].

A consistent description of the shell, pairing and collective effects can only be achieved by means of the generalized superfluid model with parameters derived on the basis of the above systematics with corresponding modifications to the pairing, asymptotic level density parameters, and moments of inertia of the saddle-point states. Differences between the asymptotic level density parameters for the fission and neutron channels are affected by the uncertainty of the surface component for the density of single-particle states. The dumb-bell saddle shapes of pre-actinides leads to the ratio $a_f/a_n > 1$ used in all analyses of fission cross sections. A value of this ratio between 1.05 and 1.07 looks the most

reasonable estimation on the basis of both the microscopic calculations and the results of fission cross-section analyses [81].

Fission input data for actinides

Highly accurate evaluations are required for the neutron-induced fission cross sections of the main fissile and fertile nuclei. Full-scale Hauser-Feshbach theory, the coupled-channel optical model, and the double-humped fission barrier parametrization are normally used in such calculations, supported by numerous experimental data that demonstrate the importance of the shell, pairing, and collective effects at both the equilibrium and saddle deformations.

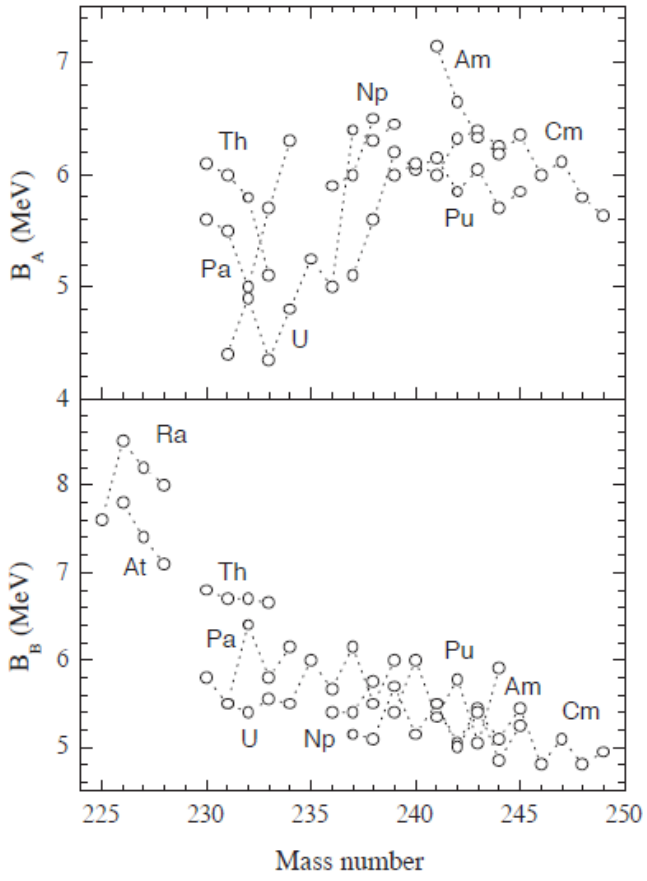

Fig. 19: Inner BA and outer BB fission barriers for actinide nuclei derived from the analysis of neutron-induced fission cross sections [421]–[425].

Fission barrier parameters corresponding to the lowest state have been estimated from modelling analyses of the available experimental data for the neutron-induced fission cross sections of the uranium, neptunium, plutonium, americium and curium isotopes [87 - 89]. Barrier parameters for Th and Pa nuclei were also obtained by adopting essentially the same approach [90, 91]; however, these specific data were less accurately estimated due to the more complex structure of the fission barriers in light actinides as compared to transuranium nuclei. The inner and outer fission barrier heights are shown in Fig. 19. A comparison between these data and the fission barriers evaluated in Ref. [92] shows that there is good agreement for the outer barriers of the uranium, plutonium and americium isotopes. Some disagreements exist for the inner barrier heights, although the general isotopic dependences are very similar; furthermore, significant discrepancies occur in the case of the outer barriers of the curium isotopes.

An empirical set of double-humped fission barrier parameters for the most important actinides containing the heights, widths and nuclear shape symmetries corresponding to the inner and the outer humps, together with the pairing correlation energies used in level density calculations are given in the *fission/empirical-barriers.dat* file [3].

The parameters of the fundamental fission barrier are strongly related to the transition-state level densities. Even in the case of fertile nuclei for which the threshold behaviour of the fission cross section provides a relatively clear signature of the barrier height, the barrier determination remains sensitive to the NLD adopted. The level density formulation and the associated parameters used in the analysis to provide the fission barrier parameters are described in the RIPL-1 Handbook [1]. Many of the analyses of fission cross sections mentioned above did not exceed 20 MeV incident energy.

According to the general concepts of the shell correction method, the double-humped structure of any fission barrier should disappear at higher excitation energies, and liquid-drop fission barriers with

asymptotic level density parameters should be used to describe both the fission cross section and all competitive reaction cross sections at excitation energies above 30–50 MeV. This prediction would appear to be supported by the available experimental data [82, 86], although there are difficulties separating unambiguously the first-step fission of an initial nucleus from the multi-chance fission of daughter nuclei that arise after the emission of one or more nucleons. So, we have only theoretical estimates of the excitation energy at which the transition from shell to liquid-drop model behaviour should occur, and lack a satisfactory understanding of what approximations should be applied to define the fission barriers and fission level densities in the transitional regime.

The quantum structure of the fission channels at the top of each barrier is extremely important in the formulation of accurate descriptions of the fission cross sections at the sub-barrier and near-barrier energies. Such structure depends strongly on the symmetry of nuclear deformations at the corresponding saddle-point states. Shell model calculations have been undertaken by many authors since the early days of fission studies. The fissioning actinide nucleus has been calculated to possess axial asymmetric shape (triaxial with mirror symmetry) at the inner saddle, and axial-symmetric and mirror-asymmetric shape at the outer saddle. Mirror-asymmetric even-even nuclei have saddlepoint rotational band levels with K^{π} = 0+, J= 0, 2, 4, … that are almost degenerate in energy with the octupole band levels K^{π} = 0−, J= 1, 3, 5, ... Therefore, the lowest rotational band at outer saddle deformation includes levels with all possible values of angular momentum and parity. A similar situation arises for triaxial shapes and levels of the °-vibrational band. The situation is even more complex for odd and odd-odd fissioning nuclei: the quantum number of the corresponding rotational bands should be estimated in accordance with the angular momentum addition rules for unpaired particles and the corresponding rotational bands. As a result, the fission cross section analysis involves a much more complex structure of saddle transition states than the well-studied collective level sequences of the deformed rare-earth nuclei and actinides at low excitation energies.

The difference between modelling the densities of the transition states and the normal states is that in the first case there are no experimental data available for normalization. Therefore, the starting values of the parameters entering the transition state density are obtained by using physical arguments to adjust the parameters of the normal states at equilibrium deformation for the saddle point deformation. The final values are deduced from the fit of the experimental data for neutron-induced fission cross sections. The calculation of the level densities for the transition states at the hump i requires beside a shape symmetry estimation also a knowledge of the shell corrections and of the damping of the shell and collective effects. All these quantities are interrelated and depend on their corresponding values for the equilibrium deformation; therefore, it is difficult to provide a general prescription for their calculation.

The shell corrections at saddle points recommended in RIPL-2 were derived from the analysis of fission cross sections in the first plateau region above the fission threshold, using the phenomenological version of GSM. Their values in MeV for the inner and the outer barriers were calculated according to:

$$\delta E_A = \begin{cases} 2.6 & Z \le 97 \\ 2.6 - 0.1(Z - 97) & Z > 97 \end{cases}$$

$$\delta E_B = \begin{cases} 0.6 + 0.1(Z - 97) + 0.04(N - 143) & Z < 97 \\ 0.6 + 0.04(N - 143) & Z \ge 97 \end{cases}$$

For the pairing correlations, RIPL-2 recommends the parametrizations $\Delta_f = \Delta_0 + 0.2$ MeV, where Δ_0 is the pairing for the neutron channels [2]. These values were also deduced from the fit to the experimental neutron-induced fission cross sections.

It should be noted that the uncertainty of the above estimates is significant [92], both for the pairing parameter and shell corrections at saddle points. The damping of the shell effects at saddle points particularly influences the shape of the first-chance fission cross section at excitation energies above

the fission threshold (i.e., in the “fission plateau”). The shell-effect damping parameter used for equilibrium deformation should be slightly adjusted to fit the experimental value of the fission cross sections.

Extensive fission-cross-section calculations for a significant number of actinides have been performed using the EGSM for both normal and transition states. For the transition states the above recommendations have been adopted. All the remaining parameters, including the moments of inertia, have been calculated by replacing the equilibrium deformation with the deformations corresponding to the saddle points. A reasonably good global description of the experimental fission cross section was obtained by adjusting only the damping of the shell correction with a factor of 0.5, and the vibrational enhancement with a factor of 2. As an example, the results of such calculations are shown in Fig. 20 in a comparison with the corresponding experimental data. More detail consideration of the calculations is presented in Ref. [4].

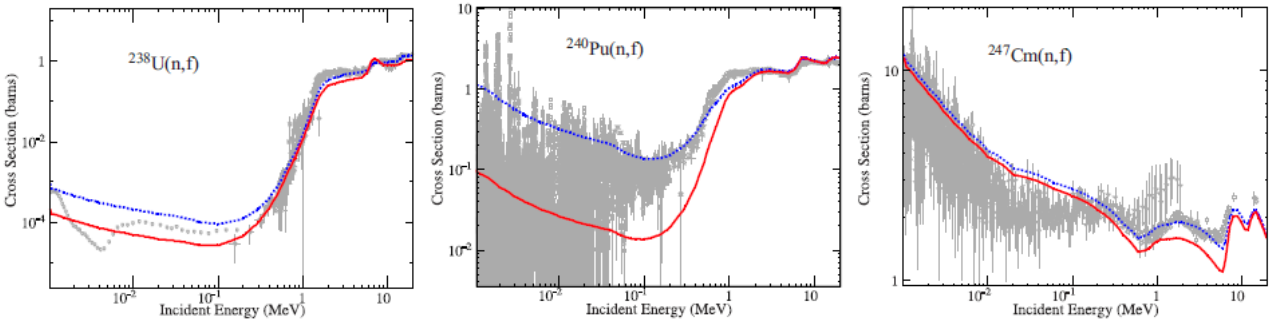

FIG. 20. Neutron induced fission cross sections of some actinides calculated with empirical ingredients recommended in RIPL (solid red line) and the adjusted parameters as described in [4] (dotted blue line). Experimental data were retrieved from the EXFOR library.

Microscopic fission barriers and level densities

Among the non-energy nuclear applications which require estimates of a large number of fission data, the most important is the stellar nucleosynthesis of the rapid neutron-capture process (or r-process) invoked to explain the origin of approximately half of the stable nuclides heavier than iron that are observed in nature. To calculate the changes in abundance of the heavy nuclei as a result of the high neutron fluxes and high temperatures encountered during the r-process nucleosynthesis, a nuclear reaction network including all neutron captures, photodisintegrations, β-decays, as well as β-delayed processes, fission processes and α-decays must be used. The fission processes include spontaneous, β-delayed and neutron-induced fission, the probabilities of which must be estimated for some 2000 nuclei with $80 < Z < 110$ mainly located in the neutron-rich region of the nuclear chart.

For these specific applications, a compilation was included in RIPL-2 containing the fission barriers for some 2301 nuclei with $78 < Z < 120$ derived using the ETFSI method and the corresponding NLDs at both saddle point deformations predicted by the microscopic model of NLD. More details are given in the RIPL-2 Handbook [2].

A set of fission paths obtained by the Hartree-Fock- Bogolyubov (HFB) calculations and corresponding nuclear level densities (NLDs) at the fission saddle points from the HFB combinatorial model are provided in table format in RIPL-3. These two nuclear ingredients are strongly interdependent and are determined coherently, the NLD being estimated from the single-particle scheme and pairing strength of the same mean field model HFB- 14 that was used to determine the fission saddle points.

The HFB model has proven capacity to estimate the *static* fission barrier height with a relatively high degree of accuracy. In particular, the barriers determined within the HFB-14 model [8] (see also chapter MASSES) reproduce the 52 primary empirical barriers (i.e., the highest barriers of prime

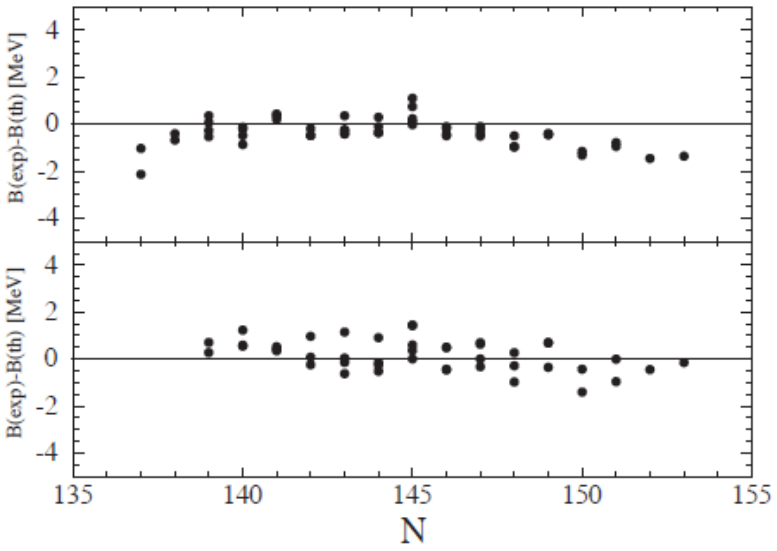

Fig. 21. Deviations between empiri-cal and HFB-14 highest (top panel) and second highest (bottom panel) barriers for actinide nuclei with $88 < Z < 96$.

interest in cross-section and decay calculations) of nuclei with $88 < Z < 96$, which are always less than 9 MeV in height, with an *rms* deviation as low as 0.67 MeV. A similar accuracy is obtained (0.65 MeV) for the secondary barriers (i.e., the second highest barriers). The empirical HFB-14 barriers are compared in Fig. 21, where differences up to 1 MeV on the highest barrier can be observed. Such a large difference obviously has a significant impact on cross section calculations, but at this stage, no theoretical models can claim to provide predictions of barrier heights with a global accuracy better than 0.5–1 MeV (in the best case). The HFB-14 model usually overestimates the height of the primary barrier, so that a global decrease of the energy surface may be required. The HFB combinatorial method developed to estimate the NLD at ground-state deformation has been used to calculate the NLD coherently at the saddle points, making use of the corresponding HFB predictions for the single-particle level scheme and pairing strength at the corresponding deformation. For many nuclear physics applications a renormalization procedure of the NLDs based on experimental data is required, in particular for nuclear data evaluation or for an accurate estimate of reaction cross sections. Though the HFB combinatorial NLDs at the saddle and isomeric deformations are provided in a tabular format, it is possible to renormalize them using Eq. (21), as was also suggested for the ground-state NLDs. The energy shift p and the scaling factor c are free parameters which can be adjusted at each saddle or isomer deformation to optimize the fit to the fission cross section. These parameters can be expected to reach values similar to those derived for the ground-state NLD, i.e., typically ±1 MeV for p and ±0.5 MeV−1/2 for c. These values reflect the remaining uncertainties in the NLD predictions on the basis of the mean-field combinatorial approach.
Selected fission cross-sections of several isotopes of U, Pu, Am and Cm were calculated using both the full fission path and the corresponding parabolic approximation; calculations were compared to available experimental data from the EXFOR library. Some results of these studies have been published [93]. The main conclusion of such sensitivity studies is that the description of the experimental data usually requires a decrease of the barrier heights and a decrease of the transition-state level density at high energies. The results also show that the uncertainty in the fission path, and more specifically in the barrier heights, gives rise to a cross section that can hardly be estimated better than within a factor of roughly 10 for energies below a few MeV. This corresponds to a 0.5–1.0 MeV error in the fission barrier height obtained from the HFB-14 model that cannot be expected to be significantly improved in the near future. Therefore, the predictive power of fission cross-section calculations based on HFB inputs remains limited.

CONCLUSION

A long-standing problem of how to meet nuclear data needs of the future with limited experimental resources puts a considerable demand upon computational nuclear modelling capabilities. Originally

almost all nuclear data were provided by measurement programmes. Over time, theoretical understanding of nuclear phenomena has reached a considerable degree of reliability, and nuclear reaction modelling has become a standard practice in nuclear data evaluation (with measurements remaining critical for data testing and benchmarking). Theoretical calculations have become instrumental in obtaining complete and internally consistent nuclear data files.

The practical use of nuclear model codes requires considerable numerical input that describes properties of the nuclei and their nuclear reactions. Experts in leading nuclear data centers have used a variety of different input parameter sets, often developed over many years in their own laboratories. Many of these partial databases were poorly documented, or not documented at all, and not always available for other users. With the trend of reduced funds for nuclear data evaluations, there was a real threat that the immense accumulated knowledge of input parameters and related state-of-the-art might be compromised or even lost for future applications. Therefore, the IAEA has undertaken an extensive coordinated effort to develop a library of evaluated and tested nuclear-model input parameters.

Nuclear data evaluators around the world have emphasized and recognized the importance of the IAEA RIPL databases, and have continued to stress their full reliance on the IAEA RIPL-2 and 3 databases for reaction cross section calculations in many publications and conference presentations.

Most of the results compiled in the RIPL database, and discussed in this contribution, have been published elsewhere. We suggest that the original work be quoted, while stating that the actual data or code used have been taken from the RIPL database (reference to a RIPL index, if relevant, should be made – see the optical model chapter for examples).

Last but not least, we would like to stress that the IAEA Nuclear Data Section will maintain in the foreseeable future both the RIPL coordination activities and the compilation of input parameters, including updates to the released RIPL-3 database. There are still large uncertainties in modelling important nuclear reactions, where insufficient experimental data for guidance exist – e.g. fission and nuclear reactions on excited states, and isomer production, to mention a few. These outstanding issues should be the subject of further activity, and could lead to further improvements in practical calculations.

At the end I would like to express my sincere acknowledgments to all colleagues who have contributed to and worked on the RIPL project during the last fifteen years. The preparation of this paper would not have been possible without the support, hard work and endless efforts of a large number of individuals and institutions.

References

1. P. Oblo˘zinsk´y, M.B. Chadwick, T. Fukahori, A.V. Ignatyuk, S. Kailas, J. Kopecky, G. Molnar, G. Reffo, Z. Su, M. Uhl, P.G. Young, O. Bersillon, E. Betak, R. Capote and V.M. Maslov, “Handbook for Calculations of Nuclear Reaction Data: Reference Input Parameter Library)”, Tech. Rep. IAEA-TECDOC-1034, International Atomic Energy Agency, Vienna, Austria, 1998 (see *http://www-nds.iaea.org/ripl/*).
2. T. Belgya, O. Bersillon, R. Capote, T. Fukahori, Zhigang Ge, S. Goriely, M. Herman, A.V. Ignatyuk, S. Kailas, A. Koning, V. Plujko and P. Young, “Handbook for calculations of nuclear reaction data, Reference Input Parameter Library- 2”, Tech. Rep. IAEA-TECDOC-1506, International Atomic Energy Agency, Vienna, Austria, 2006 (see *http://www-nds.iaea.org/RIPL-2/*).
3. T. Belgya, R. Capote, S. Goriely, M. Herman, S. Hilaire, A.V. Ignatyuk, A. Koning, V. Plujko, M. Avrigeanu, T. Fukahori, O. Iwamoto, M. Sin, E.S. Soukhovitskii, P. Talou and Y. Han, “Handbook for calculations of nuclear reaction data, Reference Input Parameter Library-3”, IAEA Tech. Rep., International Atomic Energy Agency, Vienna, Austria, to be published (see *http://www-nds.iaea.org/RIPL-3/*).
4. R. Capote, M. Herman, P. Oblo˘zinsk´y, P.G. Young, S. Goriely, T. Belgya, A.V. Ignatyuk, A. Koning, S. Hilaire, V. Plujko, M. Avrigeanu, O. Bersillon, M.B. Chadwick, T. Fukahori, Zhigang Ge, Yinlu Han, S. Kailas, J. Kopecky, V.M. Maslov, G. Reffo, M. Sin, E.S. Soukhovitskii, P. Talou and Y. Han. RIPL -

Reference Input Parameter Library for Calculations of Nuclear Reactions and Nuclear Data Evaluations, Nucl. Data Sheets, **110** (2009) 3107-3214.
5. G. Audi, A.H. Wapstra and C. Thibault, "The AME2003 atomic mass evaluation (II). Tables, graphs and references", Nucl. Phys. A729, 337-676 (2003).
6. P. Moller, J.R. Nix, W.D. Myers and W.J. Swiatecki, "Nuclear ground-state masses and deformations", At. Data Nucl. Data Tables 59, 185-381 (1995).
7. S. Goriely, F. Tondeur and J.M. Pearson, "A Hartree-Fock nuclear mass table", At. Data Nucl. Data Tables 77, 311-381 (2001).
8. S. Goriely, M. Samyn and J.M. Pearson, "Further explorations of Skyrme-Hartree-Fock-Bogoliubov mass formulas. VII. Simultaneous fits to masses and fission barriers", Phys. Rev. C75, 064312-064312.7 (2007).
9. S. Goriely, M. Samyn, P.-H. Heenen, J.M. Pearson and F. Tondeur, "Hartree-Fock mass formulas and extrapolation to new mass data", Phys. Rev. C66, 024326 (2002).
10. J. Duflo and A. Zuker, "Microscopic mass formulas", Phys. Rev. C52, R23-R27 (1995).
11. W.D. Myers and W.J. Swiatecki, "Nuclear properties according to the Thomas-Fermi model", Nucl. Phys. A601, 141-167 (1996).
12. Y. Aboussir, J.M. Pearson, A.K. Dutta and F. Tondeur, "Nuclear mass formula via an approximation to the Hartree-Fock method", At. Data Nucl. Data Tables 61, 127-134 (1995).
13. M. Herman, R Capote, B.V. Carlson, P. Oblo˘zinsk´y, M. Sin, A. Trkov, H. Wiencke and V. Zerkin, "EMPIRE: Nuclear Reaction Model Code System for Data Evaluation", Nucl. Data Sheets. 108, 2655-2715 (2007).
14. A.J. Koning, S. Hilaire and M. Duijvestijn, "TALYS-1.0", in: Proc. Int. Conf. Nuclear Data for Science and Technology, 22-27 April 2007, Nice, France, O. Bersillon, F. Gunsing, E. Bauge, R. Jacqmin, S. Leray (Eds.), EDP Sciences, 2008, Vol. 1, pp. 211-214. See also "TALYS-1.0: A nuclear reaction program", User Manual, NRG/CEA, December 2007.
15. S.F. Mughabghab, M. Divadeenam and N.E. Holden,"Neutron Cross Sections ", Vol. 1, part A, Academic Press, New York - London, 1981. S.F. Mughabghab, Vol. 1, part B, 1984.
16. T.S. Belanova, A.V. Ignatyuk, A.B. Pashchenko and V.I. Plyaskin, "Radiative Neutron Capture - Handbook", Energoatomizdat, Moscow, 1986 (in Russian).
17. S.F. Mughabghab, "Atlas of Neutron Resonances", Elsevier, Amsterdam - Tokio, 2006.
18. J. Raynal, "Optical model and coupled-channel calculations in nuclear physics", in: Computing as a language of physics, ICTP International Seminar Course, Trieste, Italy, 1971, International Atomic Energy Agency, Vienna, Austria, 1972, p. 281.
19. O. Bersillon, "SCAT2 - Un programme de mod`ele optique sph´erique", Commissariat `a l'´Energie Atomique report CEA-N-2227, 1978; Proc. ICTP Workshop on Computation and Analysis of Nuclear Data Relevant to Nuclear Energy and Safety, Trieste, Italy, 1992.
20. E.Sh. Soukhovitski, S. Chiba, R. Capote, J.M. Quesada, S. Kunieda and G. Mororovskij, "Supplement to OPTMAN Code, Manual Version 10", JAERI-Data/Code 2008-025 (Japan Atomic Energy Agency, 2008).
21. A.J. Koning and J.P. Delaroche, "Local and global nucleon optical models from 1 keV to 200 MeV", Nucl. Phys. A713, 231-310 (2003).
22. E.D. Arthur, "Parameter determination and application to nuclear model calculations of neutron-induced reactions on yttrium and zirconium isotopes", Nucl. Sci. Eng. 76, 137-147 (1980).
23. Zhigang Ge, China Nuclear Data Center, Communication of Nuclear Data Progress 21, 35 (1999), and other references in Annex 5.D of [2].
24. S. Igarasi, JAERI-M 5752, 1974, and other references in Annex 5.D of [2].
25. A.M. Lane, "New Term in the Nuclear Optical Potential: Implications for (p,n) Mirror State Reactions", Phys. Rev. Lett. 8, 171-172 (1962).
26. A. Trkov, R. Capote, I. Kodeli and L. Leal, "Evaluation of Tungsten Nuclear Reaction Data with Covariances", Nucl. Data Sheets 109, 2905-2909 (2008).
27. H. Bethe, "Nuclear Physics B. Nuclear Dynamics, Theoretical", Rev. Mod. Phys. 9, 69-244 (1937).
28. A. Gilbert and A.G.W. Cameron, "A composite nuclearlevel density formula with shell corrections", Can. J. Phys. 43, 1446-1496 (1965).

29. S. Goriely, “A new nuclear level density formula including shell and pairing correction in the light of a microscopic model calculation”, Nucl. Phys. A605, 28-60 (1996).
30. A.V. Ignatyuk, V.S. Stavinsky, Yu.N. Shubin, A.V. Ignatyuk, V.S. Stavinskii and Yu.N. Shubin, “Density of excited states of atomic nuclei” (in Russian), Nuclear Data for Reactors, Tech. Rep. STI/PUB/259, IAEA, Vienna, 1970, pp.885-907.
31. A.V. Ignatyuk, *Statistical Properties of Excited Atomic Nuclei (Russian)*, Energoatomizdat, Moscow, 1983; Translated by IAEA, *Report INDC-233(L),* Vienna, 1983.
32. S. Goriely, “A new nuclear level density formula including shell and pairing correction in the light of a microscopic model calculation”, Nucl. Phys. A605, 28-60 (1996).
33. A.V. Ignatyuk, G.N. Smirenkin and A.S. Tishin, “Phenomenological description of the energy dependence of the level density parameter”, Yad. Fiz. 21, 485-490 (1975) (in Russian).
34. W. Dilg, W. Schantl, H. Vonach and M. Uhl, “Level density parameters for the back-shifted Fermi gas model in the mass range 40 < A < 250”, Nucl. Phys. A217, 269-298 (1973).
35. A. Bohr and B. Mottelson, “Nuclear Structure”, vol 2, Benjamin Inc., New York and Amsterdam (1974).
36. J. Bardeen, L. Cooper and J. Schriffer, “Theory of superconductivity”, Phys. Rev. 108, 1175-1204 (1957).
37. A.V. Ignatyuk, G.N. Smirenkin and A.S. Tishin, “Phenomenological description of the energy dependence of the level density parameter”, Yad. Fiz. 21, 485-490 (1975) (in Russian).
38. O.T. Grudzevich, A.V. Ignatyuk, V.I. Plyaskin and A.V. Zelenetsky, “Consistent systematics of level density for medium and heavy nuclei”, in: Proc. Int. Conf. on Nuclear Data for Science and Technology, 30 May- 3 June 1988, Mito, Ibaraki, Japan, S. Igarashi (Ed.), JAERI, Tokai, Ibaraki, 1988, pp. 767-770.
39. A. D’Arrigo, G. Giardina, M. Herman, A.V. Ignatyuk and A. Taccone, “Semi-empirical determination of the shell correction temperature and spin dependence by means of nuclear fission”, J. Phys. G: Nucl. Part. Phys. 20, 365-376 (1994).
40. M.B. Chadwick, P. Oblo˘zinsk´y, M. Herman, *et al.*, “ENDF/B-VII.0: Next Generation Evaluated Nuclear Data Library for Nuclear Science and Technology”, Nucl. Data Sheets 107, 2931-3060 (2006).
41. P. Demetriou and S. Goriely, “Microscopic nuclear level densities for practical applications”, Nucl. Phys. A695, 95-108 (2001).
42. M. Hillman and J.R. Groover, “Shell-model combinatorial calculations of nuclear level densities”, Phys. Rev. 185, 1303-1319 (1969).
43. N. Cerf, “Combinatorial nuclear level density by a Monte Carlo method”, Phys. Rev. C49, 852-866 (1994).
44. S. Hilaire, J.P. Delaroche and M. Girod, “Combinatorial nuclear level densities based on the Gogny nucleonnucleon effective interaction”, Eur. Phys. J. A12, 169- 184 (2001).
45. E. Mainegra and R. Capote, “Nuclear state density calculations: An exact recursive approach”, Comp. Phys. Comm. 150, 43-52 (2003).
46. S. Hilaire and S. Goriely, “Global microscopic nuclear level densities within the HFB plus combinatorial method for practical applications”, Nucl. Phys. A779, 63-81 (2006).
47. S. Goriely, S. Hilaire and A.J. Koning, “Improved microscopic nuclear level densities within the Hartree-Fock- Bogoliubov plus combinatorial method”, Phys. Rev. C78, 064307-064307.14 (2008).
48. J.J. Griffin, “Statistical model of intermediate structure”, Phys. Rev. Lett. 17, 478-481 (1966).
49. V.M. Strutinsky, “On the nuclear level density in the case of an energy gap”, in: Proc. Int. Conf. Nucl. Phys., Paris, 1958, p. 617.
50. T. Ericson, “The statistical model and nuclear level densities”, Adv. Phys. 9, 425-511 (1960).
51. A.V. Ignatyuk and Yu.V. Sokolov, “Density of excited particle-hole states in the superfluid nuclear model”, Yad. Fiz. 17, 723-733 (1973) [Sov. J. Nucl. Phys. 17, 376-380 (1973)]; see also “Distribution of Excited Quasi- Particles and Average Statistical Characteristics of Nuclei”, Yad. Fiz. 19, 1229-1240 (1974) [Sov. J. Nucl. Phys. 19, 628-633 (1974)].
52. L.G. Moretto, “Thermodynamical properties of a paired nucleus with a fixed number of quasi-particles”, Nucl. Phys. A243, 77-99 (1975).
53. C. Kalbach, “Improved implementation of pairing corrections in exciton model particle-hole state densities”, Nucl. Sci. Eng. 95, 70-78 (1987).

54. F.C. Williams Jr., “Particle-hole state density in the uniform spacing model”, Nucl. Phys. A166, 231-240 (1971).
55. E. Betak and P. Hodgson, “Particle-hole state densities in pre-equilibrium nuclear reaction models”, Rep. Progr. Phys. 61, 483-524 (1998).
56. M. Avrigeanu and V. Avrigeanu, “Partial level densities for nuclear data calculations”, Comp. Phys. Comm. 112, 191-225 (1998).
57. B.A. Nemshkalo, V.K. Sirotkin and K.B. Shebeko, “Analysis of partial and total cross sections of the 48,50Ti(p,°)49,51V reactions”, Yad. Fiz. 55, 123-129 (1992) (in Russian).
58. I.D. Fedorets, “Radiative strength functions in nuclei near the dosed Z = 28 proton shell”, Yad. Fiz. 64, 51-59 (2001) (in Russian).
59. U. Kneissl, N. Pietralla and A. Zilges, “Low-lying dipole modes in vibrational nuclei studied by photon scattering”, J. Phys. G: Nucl. Part. Phys. 32, R217-R252 (2006).
60. G. Rusev, R. Schwengner, F. D¨onau, *et al.*, “Systematics of magnetic dipole strength in the stable even-mass Mo isotopes”, Phys. Rev. 73, 044308-44308.12 (2006).
61. R. Schwengner, G. Rusev, R. Beyer, *et al.*, “Dipole response of 88Sr up to the neutron-separation energy”, Phys. Rev. C76, 034321-034321.15 (2007).
62. A.P. Tonchev, C. Angell, M. Boswell, C.R. Howell, H.J. Karwowski, J.H. Kelley, W. Tornow and N. Tsoneva, “Missing dipole excitation strength below the particle threshold, in: Proc. Int. Workshop on Photon Strength Functions Rel. Topics, Prague, Czech Republic, 17-20 June 2007, Proceedings of Science PSF07, F. Be˘cv´a˘r (Ed.), PoS(PSF07)017, 2008.
63. C.M. McCullagh, M. Stelts and R.E. Chrien, “Dipole radiative strength functions from resonance neutron capture”, Phys. Rev. C23, 1394-1403 (1981).
64. J. Kopecky and M. Uhl, “Test of gamma-ray strength functions in nuclear reaction model calculations”, Phys. Rev. C41, 1941-1955 (1990).
65. F. Bechv´ar, P. Cejnar, R.E. Chrien and J. Kopecky, “Test of photon strength functions by a method of two-step cascades”, Phys. Rev. C46, 1276-1287 (1992).
66. Z. Szefli´nski, G. Szefli´nska, Z. Wilhelmi, T. Rz¸aca- Urban, H.V. Klapdor, E. Anderson, K. Grotz and J. Metzinger, “Experimental test of the Brink hypothesis”, Phys. Lett. B126, 159-163 (1983).
67. Yu.P. Popov, “Decay of highly excited states by ®- particle emission”, in: Neutron induced reactions, Proc. Europhys. Topical Conf., June 21-25, 1982, Smolenice, P. Oblozinsky (Ed.), Institute of Physics, EPRC, 1982, pp. 121-134.
68. S. Goriely and E. Khan, “Large-scale QRPA calculation of E1-strength and its impact on the neutron capture cross section”, Nucl. Phys. A706, 217-232 (2002).
69. F. Catara, E.G. Lanza, M.A. Nagarajan and A. Vitturi, “Effect of large neutron excess on the dipole response in the region of the giant dipole resonance”, Nucl. Phys. A624, 449-458 (1997).
70. I. Hamomoto, H. Sagawa and X.Z. Zhang, “Structure of giant quadrupole resonances in neutron drip line nuclei”, Phys. Rev. C55, 2361-2365 (1997); *ibid*, “Isoscalar and isovector dipole mode in drip line nuclei in comparison with ¯-stable nuclei”, Phys. Rev. C57, R1064-R1068 (1998).
71. V.A. Rodin and M.G. Urin, “Description of radiative and weak strength functions of nuclear compound states within a semimicroscopic approach”, Physics of Elementary Particle and Atomic Nuclei 31, 976-1009 (2000) (in Russian).
72. S. Goriely, “Radiative neutron captures by neutron-rich nuclei and the r-process nucleosynthesis”, Phys. Lett. B436, 10-18 (1998).
73. R.E. Chrien, in: 5th School on Neutron Physics (Alushta 1986), Dubna, JINR, 1986, p.29.
74. S.G. Thompson, “Some aspects of the study of fission”, Arkiv Fysik 36, 267-277 (1967).
75. L.G. Moretto, “Fission probabilities in lighter nuclei: A theoretical and experimental investigation of the shell and pairing effects in fissioning nuclei”, in: Proc. Third IAEA Symp. on Physics and Chemistry of Fission, Rochester, New York, 13 - 17 August 1973, Rep. STI/PUB/347, Vol. I, International Atomic Energy Agency, Vienna, Austria, 1974, pp. 329-364.

76. H. Freiesleben, H.C. Britt and J.R. Huizenga, “Energy dependence of ¡*f* /¡*n* for the nucleus 216Rn ”, Proc. Third IAEA Symp. on Physics and Chemistry of Fission, Rochester, New York, 13 - 17 August 1973, Rep. STI/PUB/347, Vol. I, International Atomic Energy Agency, Vienna, Austria, 1974, pp. 447-457.
77. A.V. Ignatyuk, M.G. Itkis, V.N. Okolovich, G.N. Smirenkin and A.S. Tishin, “Fission of Preactinide Nuclei”, Yad. Fiz. 21, 1185-1205 (1975). [Sov. J. Nucl. Phys. 21, 612-621 (1976)].
78. Yu.Tc. Oganessian and Yu.A. Lazarev, “Treatise on Heavy-Ion Science”, D. Bromley (Ed.), 1987, Vol. 4, p.3.
79. W.D. Myers and W.J. Swiatecki, “Thomas-Fermi fission barriers”, Phys. Rev. C60, 014606 (1999).
80. A.J. Sierk, “Macroscopic model of rotating nuclei”, Phys. Rev. C33, 2039-2053 (1986).
81. A.V. Ignatyuk, G.N. Smirenkin, M.G. Itkis, C.I. Mulgin, and V.N. Okolovich, “Study on the pre-actinide nuclei fissility by charged particles”, Sov. Part. Nucl. 16, 709-772 (1985) (in Russian).
82. S.E. Vigdor, H.J. Karwowski, W.W. Jacobs, S. Kailas, P.P. Singh, F. Soga and T.G. Throwe, “Decay of hot, high-spin nuclei produced in 6Li-induced fusion reactions”, Phys. Rev. C26, 1035-1067 (1982).
83. I. Halpern and V.M. Strutinsky, in: Proc. 2nd Conf. Peaceful Uses of Atomic Energy, United Nations, Geneva, Volume 15, 1958, p.408.
84. A.V. Ignatyuk, K.K. Istekov and G.N. Smirenkin, “Analysis of angular anisotropy in low-energy fission of pre-actinide nuclei”, Sov. J. Nucl. Phys. 36, 54-62 (1982).
85. A.V. Ignatyuk, K.K. Istekov, V.N. Okolovich and G.N. Smirenkin, “Level density and fission probability in spherical and deformed nuclei”, in: Proc. Int. Symp. on Physics and Chemistry of Fission, 14 - 18 May 1979, Juelich, Germany, Rep. STI/PUB/526, International Atomic Energy Agency, Vienna, Austria, 1980, Vol. 1, pp. 421-442 (in Russian).
86. A.R. Junghans, M. De Jong, H.-G. Clerc, A.V. Ignatyuk, G.A. Kudyaev and K.-H. Schmidt, “Projectile fragment yields as a probe for the collective enhancement in the nuclear level density”, Nucl. Phys. A629, 635-655 (1998).
87. V.M. Maslov and Y. Kikuchi, “Statistical model calculations of the 232U fission cross section”, Nucl. Sci. Eng. 124, 492-497 (1996).
88. V.M. Maslov, E.Sh. Sukhovitskij, Yu.V. Porodzinskij, A.B. Klepatskij and G.B. Morogovskij, “Evaluation of neutron data for curium-246”, Rep. INDC(BLR)-4, “Evaluation of neutron data for americium-241”, Rep. INDC(BLR)-5, International Atomic Energy Agency, Vienna, Austria, 1996.
89. V.M. Maslov, E.Sh. Sukhovitskij, Yu.V. Porodzinskij and G.B. Morogovskij, “Evaluation of neutron data for 242*m*Am”, Rep. INDC(BLR)-7, “Evaluation of neutron data for 238Pu”, Rep. INDC(BLR)-9, “Evaluation of neutron data for 242Pu”, Rep. INDC(BLR)-10, International Atomic Energy Agency, Vienna, Austria, 1997.
90. V.M. Maslov, “Analysis of 232Th(n,2n) reaction data”, Ann. Nucl. Energy 19, 181-183 (1992).
91. V.M. Maslov, “Evaluation of 231,232,233Pa neutron data”, Yadernye Konstanty 1, 80-82 (1992) (in Russian).
92. G.N. Smirenkin, “Preparation of evaluated data for a fission barrier parameter library for isotopes with *Z*=82-98, with consideration of the level density models used”, Rep. INDC(CCP)-359, International Atomic Energy Agency, Vienna, Austria, 1993.
93. S. Goriely, S. Hilaire, A.J. Koning, M. Sin and R. Capote, “Towards a prediction of fission cross section on the basis of microscopic nuclear inputs”, Phys. Rev. C79, 024612-024612.13 (2009).